Evaluation of the CNESTEN's TRIGA Mark II research reactor physical parameters with TRIPOLI-4® and MCNP

H Ghninou, A Gruel, A Lyoussi, C Reynard-Carette, C El Younoussi, B El Bakkari, Y Boulaich

Nuclear Engineering and Technology 55 (2023) 4447–4464

Contents lists available at ScienceDirect

Nuclear Engineering and Technology

journal homepage: www.elsevier.com/locate/net

Original Article

Evaluation of the CNESTEN's TRIGA Mark II research reactor physical parameters with TRIPOLI-4® and MCNP

H. Ghninou [a,*], A. Gruel [a], A. Lyoussi [a], C. Reynard-Carette [b], C. El Younoussi [c], B. El Bakkari [c], Y. Boulaich [c]

[a] CEA, DES, IRESNE, DER, SPESI, LP2E, Cadarache, F-13108, Saint-Paul-lez-Durance, France
[b] Aix Marseille University, Université de Toulon, CNRS, IM2NP, Marseille, France
[c] National Center for Energy Sciences and Nuclear Technology, CNESTEN, Rabat, 10001, Morocco

ARTICLE INFO

Keywords:
MCNP simulations
TRIPOLI-4 simulations
TRIGA reactor
S/U analysis

ABSTRACT

This paper focuses on the development of a new computational model of the CNESTEN's TRIGA Mark II research reactor using the 3D continuous energy Monte-Carlo code TRIPOLI-4 (T4). This new model was developed to assess neutronic simulations and determine quantities of interest such as kinetic parameters of the reactor, control rods worth, power peaking factors and neutron flux distributions. This model is also a key tool used to accurately design new experiments in the TRIGA reactor, to analyze these experiments and to carry out sensitivity and uncertainty studies. The geometry and materials data, as part of the MCNP reference model, were used to build the T4 model. In this regard, the differences between the two models are mainly due to mathematical approaches of both codes. Indeed, the study presented in this article is divided into two parts: the first part deals with the development and the validation of the T4 model. The results obtained with the T4 model were compared to the existing MCNP reference model and to the experimental results from the Final Safety Analysis Report (FSAR). Different core configurations were investigated via simulations to test the computational model reliability in predicting the physical parameters of the reactor. As a fairly good agreement among the results was deduced, it seems reasonable to assume that the T4 model can accurately reproduce the MCNP calculated values. The second part of this study is devoted to the sensitivity and uncertainty (S/U) studies that were carried out to quantify the nuclear data uncertainty in the multiplication factor k_{eff}. For that purpose, the T4 model was used to calculate the sensitivity profiles of the k_{eff} to the nuclear data. The integrated-sensitivities were compared to the results obtained from the previous works that were carried out with MCNP and SCALE-6.2 simulation tools and differences of less than 5% were obtained for most of these quantities except for the C-graphite sensitivities. Moreover, the nuclear data uncertainties in the k_{eff} were derived using the COMAC-V2.1 covariance matrices library and the calculated sensitivities. The results have shown that the total nuclear data uncertainty in the k_{eff} is around 585 pcm using the COMAC-V2.1. This study also demonstrates that the contribution of zirconium isotopes to the nuclear data uncertainty in the k_{eff} is not negligible and should be taken into account when performing S/U analysis.

1. Introduction

The National Center for Energy, Sciences and Nuclear Techniques (CNESTEN) operates a 2 MW TRIGA Mark II research reactor, which achieved its initial criticality on 02 May 2007. This type of reactor is specially designed to effectively implement the various fields of nuclear research such as Neutron Activation Analysis, education and training, Neutron Radiography [1,2], Detectors testing [3,4] and radio-isotopes production [5,6]. Over the last few years, a complete computational model [7] of the TRIGA reactor was developed using the 3-D continuous energy Monte-Carlo code MCNP [40]X-5 Monte Carlo Team, 2004) to support planning, design and implementation of new experiments within and beyond the reactor core. The MCNP simulations were then coupled with an MCNP tally-based code BUCAL-1 [8] in order to evaluate the fuel burnup of the reactor [9]. Moreover, the measurements, which were based on neutron activation technique, were carried out so

* Corresponding author.
E-mail address: hamza.ghninou@cea.fr (H. Ghninou).

https://doi.org/10.1016/j.net.2023.07.029
Received 21 November 2022; Received in revised form 15 July 2023; Accepted 23 July 2023
Available online 4 August 2023

as to characterize the neutron flux in different irradiation channels of the CNESTEN's TRIGA reactor [10]. The latter study was carried out as part of the bilateral collaboration between the French Atomic Energy and Alternative Energies Commission (CEA) and the CNESTEN. This collaboration has been established in order to accurately characterize the irradiation and instrumentation channels of the CNESTEN's TRIGA reactor. This will lead to an easily accessible reference neutron and photon field, which can be used for the test, qualification and calibration of innovative nuclear instrumentations and contribute to the improvement of nuclear data knowledge. Furthermore, it has been agreed to develop a new computational model based on the 3D Monte-Carlo TRIPOLI-4® code [11]. The purpose of this decision is to enable CEA to have a versatile calculation tool to carry out preliminary calculations that are essential to a precise preparation for new neutron and photon measurement campaigns in the TRIGA reactor and to elaborate interpretation of these measurements. The work conducted during this collaboration will also allow the improvement and the validation of the computational models of the reactor by carrying out an in-depth analysis of the conducted experiments. Besides, a critical analysis of the computational models will be performed aiming to improve their performance with regard to the important parameters during the qualification of nuclear instrumentation (absolute neutron and photon flux levels, neutron and photon spectra, nuclear heating …).

In this study, we present a new computational model of the CNESTEN's TRIGA reactor developed with the Monte-Carlo TRIPOLI-4.11 code. This simulation code was chosen based on its general geometry modelling capability, correct representation of particles transport and continuous-energy cross sections treatment. The analysis presented in this study focuses on the calculation of the kinetic criticality parameters (k_{eff}, β_{eff}, Λ_{eff}), the control rods reactivity worth, the power peaking factors and neutron flux. In order to perform this analysis, the obtained results are compared with MCNP and experimental results available in the Final Safety Analysis Report (FSAR) of the TRIGA reactor. This study deals also with sensitivity calculations in order to derive the nuclear data uncertainty in the k_{eff} value. In this manner, the new T4 model was used to carry out the k_{eff} sensitivity profiles for different nuclide-reactions that are of central importance for the TRIGA reactor concept. Based on that sensitivity profiles and by using the COMAC-V2.1 covariance matrices database [12] we were able to quantify the nuclear data uncertainties in the k_{eff} of the TRIGA reactor.

For this study, we shall start by providing a general description of the reactor and the associated TRIPOLI-4 computational model (cf. sections 3.1 and 3.2); then, we will focus on the comparisons for two core configurations (cf. sections 4.1, 4.2, 4.3 and 4.4); after that, we will delve into the k_{eff} sensitivity analysis and uncertainty quantification (cf. section 4.5); and at last, and for every part of this article, the obtained results are discussed.

2. Reactor description and computational model

2.1. Reactor description

The Moroccan TRIGA (Training Research and Isotope production General Atomics) Mark II is a pool type light water cooled and moderated reactor using low-enriched uranium fuel that typically operates at a steady state power up to 2 MW. The fuel material consists of a uniform mixture of uranium (8.5 %wt, enriched to 19.7% of ^{235}U), hydrogen and zirconium. The reactor core is submerged in a light water pool of 2.5 m diameter and 8.8 m height. Fig. 1 presents the reactor core assembly, which is composed of 7 concentric rings labelled from A (central thimble) to G which hold a total of 101 fuel elements (FEs), including 5 fuel-follower control rods (FFCR), 17 graphite elements, a central thimble (CT) and a pneumatic transfer system (PTS). The latter can quickly transfer samples between the radiochemistry lab and the in-core irradiation position and it is used to irradiate and transport samples with short half-lives. The reactor is also equipped with a rotary specimen rack (RSR) containing 40 irradiation positions, which allow the irradiation of long half-life specimens. Besides, the Moroccan TRIGA reactor is equipped with a thermal column and four beam ports channels penetrating the concrete shield, the aluminum tank and the reactor tank. Beam port NB1 is a tangential port, whereas beam ports NB2, 3 and 4 are radially oriented ports (cf. Fig. 3). These tubes allow the neutron and gamma beams to pass from the reactor core to the outside of the reactor shield structure for experiments.

As mentioned above, the FE is a solid homogeneous mixture of U–ZrH, with a 1.6 atomic ratio between zirconium and hydrogen. The entire active fuel part is encased in a stainless steel cylindrical can of 0.05 mm thickness and an outside diameter of 37.6 mm. The top and the

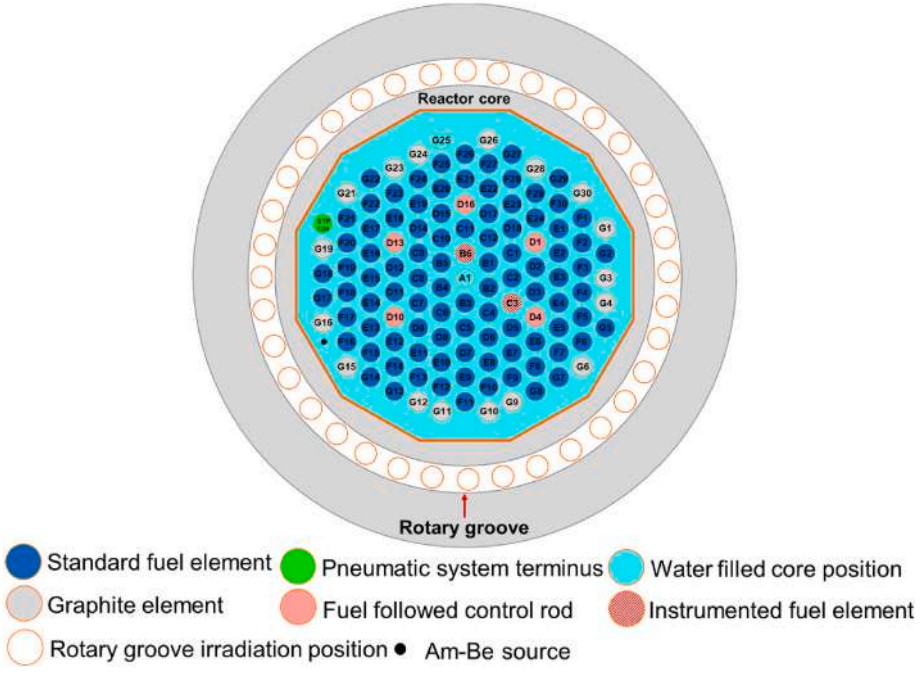

Fig. 1. The current operating configuration of the CNESTEN's TRIGA reactor.

bottom parts of the FE are made up of two cylindrical graphite plugs, leading to local neutron reflection and thermalization.

The adjustment and control of reactor power during steady-state operation is accomplished by five fuel-follower control rods (FFCR), positioned in D1, D4, D10, D13 and D16 as shown in Fig. 1. The absorbing part of the rod is filled with boron carbide (B_4C), that contains ^{10}B, which is an excellent thermal neutron absorber with high absorption cross section of thermal neutrons ($\sigma = 3843$ b). The lower part of the FFCR contains U–ZrH fuel that has the same characteristics of that of a standard FE. Depending on whether the control rod is inserted or withdrawn, it modifies the distribution of thermal neutron in the reactor core, and thus changing the value of k_{eff} which results in a change of the core reactivity (cf. Fig. 2).

2.2. TRIPOLI modelling of TRIGA MARK II reactor

The new T4 computational model of the CNESTEN's TRIGA reactor was developed based on the same geometry and materials data that were used to develop the MCNP reference model. Therefore, the relative differences between the two models are only due to the mathematical approaches used in both codes. Fig. 3 provides radial and axial views of the reactor core, and shows the main aspects of the model's geometry. As it can be seen, the reactor core and all the irradiation facilities have been accurately modelled with full available precision, meaning that the zirconium rod, stainless steel cladding and endcaps, air gaps and molybdenum supporting disc are explicitly described. Furthermore, the supporting grids, graphite reflector, annular lead bloc, thermal column, rotary groove and beam ports are also taken into account in this model.

2.3. Investigated TRIGA's core configurations

Two core configurations were investigated via simulations to test the computational model reliability in predicting the physical parameters of the reactor. As shown in Fig. 4, these configurations are denoted as:

- **C-101**: 101 FE, FFCR fully withdrawn, which corresponds to the operating configuration at full steady-state power of the core.
- **C-96**: 96 FE, FFCR fully inserted, corresponding to the subcritical configuration when the reactor is shut down.

For both configurations we calculated the kinetic parameters (k_{eff}, β_{eff} and Λ_{eff}) of the TRIGA reactor that were then compared to MCNP and experimental results. The power peaking factors (f_{HR}, f_Z and f_R), the control rods reactivity worth and the neutron flux distributions were only calculated for the C-101 configuration.

With both MCNP and T4, criticality calculations were performed using the nuclear data libraries based on ENDFB-VII.1 (ENDFB7R1) evaluation [13] at 300 K taking into account the $S(\alpha,\beta)$ thermal scattering cross-sections of bounded nuclei (i.e. H in H_2O, C in graphite, Zr in ZrH and H in ZrH) that are important to simulate the neutron interactions at energies around 4 eV. Moreover, the nuclear data library JEFF3.1.1 [14] was also used for comparison purposes, to study the impact on calculated kinetic parameters.

3. Results and discussions

3.1. Kinetic parameters of the reactor

In order to be qualitatively compared, different set of calculations were precisely defined, meaning that the type of scores and tallies, the position of scoring volumes as well as the number of simulated neutrons are defined in the same way between both codes. The calculations were then run separately with T4 (at the CEA) and MCNP (at the CNESTEN). Table 1 presents the calculated k_{eff} values for the two considered core configurations. The comparison shows a good agreement between T4 and MCNP results. The differences, in terms of (T4 - MCNP), for the ENDFB7R1 are around 144 ± 4 pcm and 52 ± 4 pcm for C-101 and C-96 core configurations, respectively. Since both models are defined in exactly the same way, the discrepancies are due to the different approaches and methods implemented in the two codes, in particular the different approaches used to treat the region of unresolved resonances especially for inelastic scattering reactions. In T4, the neutron cross sections in the unresolved resonance range are generated by the CALENDF [15] code. The latter converts resolved and unresolved resonance parameters into temperature-dependent continuous energy cross sections, and then generates the probability tables that are used by T4 simulations. Whereas, for MCNP, the neutron cross section in the unresolved resonance range is directly sampled from the probability tables. Besides, the differences can also be attributed to the different estimators used by both codes. It is also worth mentioning that the comparison between k_{eff} values, calculated with T4 ENDFB7R1 and JEFF3.1.1 cross section libraries, has shown that the JEFF3.1.1 slightly over-estimates the k_{eff} by around 192 ± 6 pcm and 163 ± 6 pcm for both C-101 and C-96 configurations, respectively as compared to ENDFB7R1. This discrepancy can be related to the differences between the ENDFB7R1 and JEFF3.1.1 cross section data libraries.

The knowledge of the effective delayed neutron fraction β_{eff} [1] and the mean neutron generation time Λ_{eff}, is for a high interest in reactor kinetics. For TRIGA type reactors, these parameters are generally given by the manufacturer and are not evaluated for different core configurations. For a TRIGA Mark II reactor with a low enriched uranium (LEU) fuel under than 20% ^{235}U enrichment, the recommended values of β_{eff} and Λ_{eff} are 700 pcm and 31 μs, respectively (Negut et al., 2006). Besides, it has been shown that the kinetic parameters of the TRIGA reactor strongly depend on the fuel type and core configuration [16]. Hence, it was decided to calculate the β_{eff} and Λ_{eff} values with both T4 and MCNP in order to be able to evaluate the discrepancies between both models. There are different methods for the calculation of the kinetic parameters:

- The first method is based on the "Iterated Fission Probability" (IFP) [17]. It allows to calculate the kinetic parameters of the reactor weighted by the adjoint flux. This method is implemented in both T4 [18] and MCNP [19] codes.
- The second method, called the "NAUCHI method" [20], which is a first order approximation of the IFP method. This method allows to calculate the kinetic parameters and it is implemented in T4 and MCNP-4C codes, but not in MCNP5 which was used in this study.
- Another method for the calculation of β_{eff}, which is called the "prompt method" (also referred to as k-ratio) [21], requires two calculations. In the first calculation, we evaluate the k_{eff} taking into account the contribution of both prompt and delayed neutrons. Then, we perform a second calculation of the multiplication factor (k_p) taking into account only the contribution of the prompt neutrons. The value of β_{eff} is then given by the following equation:

$$\beta_{eff} = 1 - \frac{k_p}{k_{eff}} \qquad \text{Eq. 1}$$

The results of the calculation of β_{eff} with T4 and MCNP (IFP method) using the ENDFB7R1 nuclear data library are presented in Table 2. The results show a good agreement with a maximum relative difference of 0.6% ± 0.4% for the C-101 core configuration. On the other hand, the impact of cross section libraries on the estimation of the β_{eff} value is also studied. As reported in Table 2, the JEFF3.1.1 data library overestimates, as compared to ENDFB7R1, the β_{eff} by around 16 pcm.

[1] These values are called effective when the mean β and Λ values are weighted by the adjoint flux.

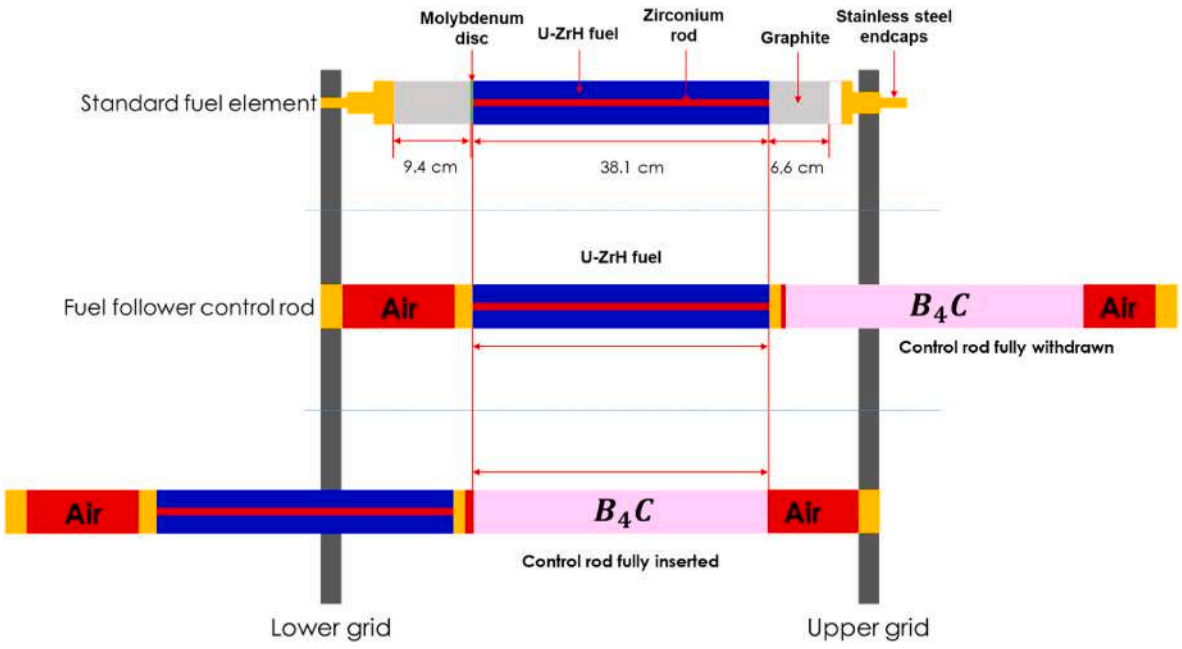

Fig. 2. Schematic of the FFCR when fully inserted and withdrawn from the reactor core.

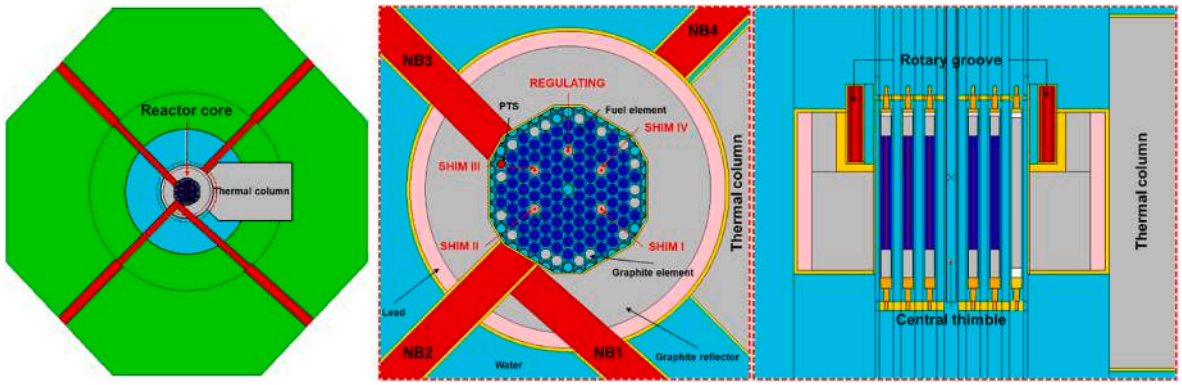

Fig. 3. Radial (left and middle) and axial (right) views of the TRIPOLI-4 model of the CNESTEN's TRIGA reactor in the current operating configuration.

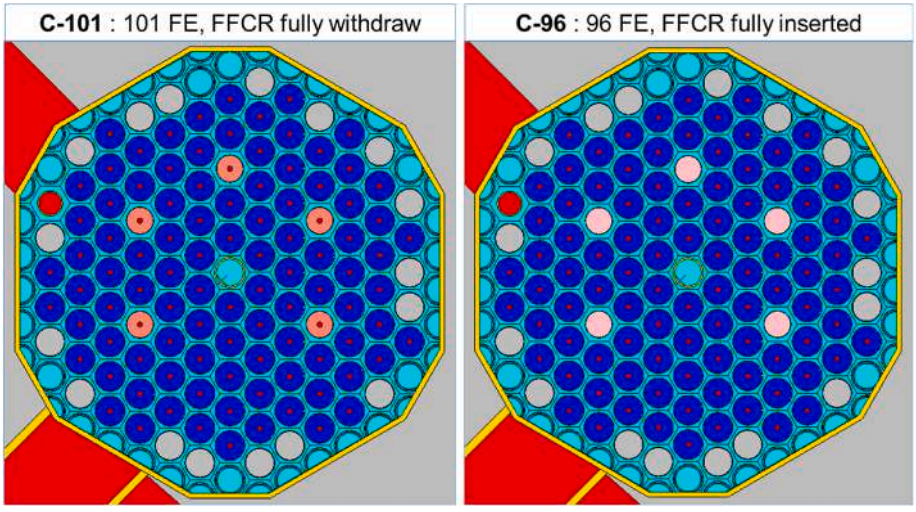

Fig. 4. The investigated core configurations of the CNESTEN's TRIGA reactor.

Table 1
Comparison between the calculated k_{eff} values for two core configurations.

Core configuration	T4 – JEFF3.1.1	T4 - ENDFB7R1	MCNP - ENDFB7R1	T4 – MCNP (ENDFB7R1)
	k_{eff}	k_{eff}	k_{eff}	
C-101	1.08190 ± 4 pcm	1.07998 ± 4 pcm	1.07854 ± 2 pcm	144 ± 4 pcm
C-96	0.97005 ± 4 pcm	0.96842 ± 4 pcm	0.96790 ± 2 pcm	52 ± 4 pcm

Table 2
Comparison between the calculated β_{eff} values for two core configurations.

Core configuration	T4 – JEFF3.1.1		T4 - ENDFB7R1		MCNP - ENDFB7R1		T4/MCNP-1 IFP – ENDFB7R1
	β_{eff} (pcm) IFP	β_{eff} (pcm) NAUCHI	β_{eff} (pcm) IFP	β_{eff} (pcm) NAUCHI	β_{eff} (pcm) PROMPT	β_{eff} (pcm) IFP	
C-101	739 ± 2	728 ± 1	722 ± 2	711 ± 1	720 ± 2	718 ± 2	0.6% ± 0.4%
C-96	743 ± 2	731 ± 1	727 ± 2	713 ± 1	734 ± 2	725 ± 2	0.3% ± 0.4%

Table 3
Comparison between the calculated Λ values for two core configurations.

Core configuration	T4 – JEFF3.1.1	T4 - ENDFB7R1	MCNP - ENDFB7R1	T4/MCNP-1 ENDFB7R1
	Λ_{eff} [μs]	Λ_{eff} [μs]	Λ_{eff} [μs]	
C-101	39.2 ± 0.01	34.4 ± 0.01	33.9 ± 0.3	1.5% ± 1.1%
C-96	43.7 ± 0.02	46.1 ± 0.02	45.8 ± 0.4	0.6% ± 0.9%

Results regarding the mean neutron generation time Λ_{eff} are presented in Table 3. The Calculated values are in good agreement with a maximum relative difference of 1.5% ± 1.1% for the C-101 configuration.

From the above-presented values of k_{eff} (cf. Table 1) and taking into account the calculated β_{eff} values (cf. Table 2), we can estimate the core excess reactivity with all control rods withdrawn in $[2] unit by the following equation:

$$\rho = \frac{k_{eff} - 1}{k_{eff} \times \beta_{eff}} \quad \text{Eq. 2}$$

The comparison between the experimental, T4 and MCNP calculated core excess reactivity is shown in Table 4. The (C/E)[3] −1 relative differences are around −0.2% and −0.3% for T4, with ENDFB7R1 and JEFF3.1.1 respectively, and −1.6% for MCNP. Which indicated that both T4 and MCNP computational models can accurately reproduce the experimental results.

Table 4
Experimental and calculated values of core excess reactivity.

Core configuration	Core excess reactivity ($)		(C/E)-1
C-101	Experiment	10.27	–
	T4 – ENDFB7R1	10.25 ± 0.03	−0.2%
	T4 – JEFF3.1.1	10.24 ± 0.03	−0.3%
	MCNP – ENDFB7R1	10.11 ± 0.03	−1.6%

[2] Dollar unit refers to the reactivity divided by β_{eff}.The reactivity of a system is 1 $ if $\rho = \beta_{eff}$.

[3] 'C/E−1' refers to 'Calculation/Experiment-1', which represents the relative differences between calculation and experiment. It is important to note that 'C' can be either 'T4,' referring to 'TRIPOLI-4,' or 'MCNP'.

3.2. Control rods worth

As mentioned in section 3.1, the adjustment and control of the reactor power at steady-state operation is achieved by five FFCR. The control rod worth is calculated as follows:

- Calculation of the k_{eff} of the core with all control rods positioned in their critical position, denoted k_{eff0}.
- The control rod is withdrawn to a certain position "*i*", while keeping the other control rods at the same critical position, and we calculate the new value of k_{eff}, denoted as k_{effi}.

The integral reactivity worth of the considered control rod is obtained by comparing k_{eff0} and k_{effi} as indicated in the following formula:

$$\rho = \left(1 - \frac{1}{k_{eff0}}\right) - \left(1 - \frac{1}{k_{effi}}\right) \quad \text{Eq. 3}$$

The absolute uncertainty of ρ (in $) is determined by applying the general law of propagation of uncertainties considering that the variables are independent of each other. The uncertainty is given by the following equation:

$$u(\rho) = \left(\left(\frac{u(k_{eff0})}{\beta_{eff} {k_{eff0}}^2} \right)^2 + \left(\frac{u(k_{effi})}{\beta_{eff} {k_{effi}}^2} \right)^2 + \left(\frac{k_{effi} - k_{eff0}}{k_{eff0} \times k_{effi}} \right)^2 \left(\frac{u(\beta_{eff})}{\beta_{eff}^2} \right)^2 \right)^{1/2} \quad \text{Eq. 4}$$

Fig. 5 shows the comparisons between the calculated and experimental integral reactivity worth for all the control rods. From these curves, it can be seen that the calculated T4 and MCNP values with ENDFB7R1 library are in a good agreement. Nevertheless, the maximum relative differences, between the calculated T4 values with JEFF3.1.1 and ENDFB7R1, are around 2.5%, 5%, 3%, 2% and 3% for SHIM I, SHIM II, SHIM III, SHIM IV and REGULATING rod, respectively. By comparing the experimental and calculated curves, one can observe a reasonable agreement for SHIM I, SHIM III and SHIM II. For the latter, the relative difference increases as soon as the SHIM II control rod is withdrawn by more than 60%. In this case, the relative difference can reach its maximum when the control rod is completely withdrawn with a relative difference (T4/E−1) of −2.7% ± 1.1% and (MCNP/E−1) −6.2% ± 1.1%. For both SHIM IV and REGULATING control rods, the calculated T4 (ENDFB7R1 and JEFF3.1.1) and MCNP (ENDFB7R1) are slightly under-estimated compared with the experimental ones. Nevertheless, these results are satisfactory in comparison to some published results for other TRIGA reactors [22–24]. Table 5 reports that the experimental and calculated total reactivity worth are in good agreement for all the control rods. The maximum relative differences are around 3.3% ± 2.5% (SHIM III) and −6.2% ± 1.1% (SHIM II) for T4 and MCNP, respectively.

The shutdown margin (SDM) of the TRIGA reactor is expressed in terms of reactivity and can be defined as the total control rod reactivity worth minus the excess reactivity in the core when all the control rods are completely withdrawn. In other words, the SDM is the amount of reactivity needed to bring the reactor to its critical operating condition. The SDM for C-101 core configuration of the TRIGA reactor was calculated and the results are reported in Table 6. As it can be seen, the calculated SDM values are in good agreement with the experimental

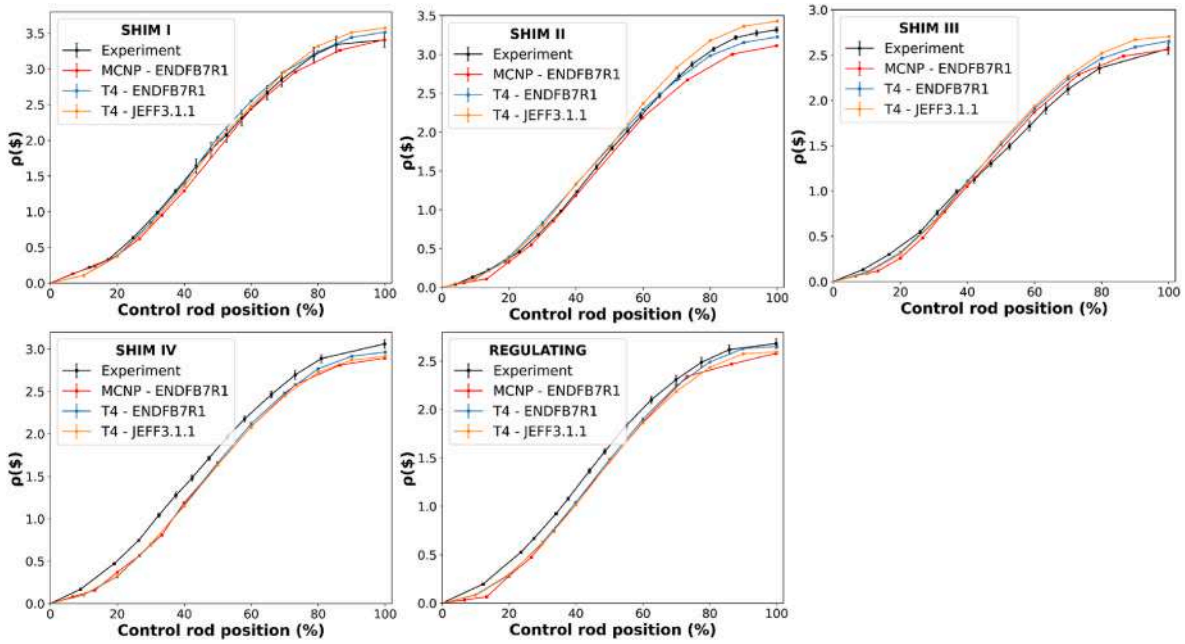

Fig. 5. Comparison between the calculated, T4 and MCNP, and experimental integral control rods worth.

Table 5
Comparison between the calculated and measured total control rods reactivity worth (ENDFB7R1).

Control rod worth in ($)					
Control rod	Experiment	T4 - ENDFB7R1	MCNP - ENDFB7R1	T4/E−1	MCNP/E−1
SHIM I	3.4 ± 0.1	3.5 ± 0.001	3.4 ± 0.001	3.2% ± 3.1%	0.1% ± 3.1%
SHIM II	3.3 ± 0.1	3.2 ± 0.001	3.1 ± 0.001	−2.7% ± 1.1%	−6.2% ± 1.1%
SHIM III	2.6 ± 0.1	2.7 ± 0.001	2.6 ± 0.001	3.3% ± 2.5%	−0.4% ± 2.4%
SHIM IV	3.1 ± 0.1	3.0 ± 0.001	2.9 ± 0.001	−3.2% ± 1.6%	−5.5% ± 1.6%
REGULATING	2.7 ± 0.1	2.7 ± 0.001	2.6 ± 0.001	−1.1% ± 1.9%	−3.8% ± 1.8%
Total	15.1 ± 0.2	15.0 ± 0.002	14.6 ± 0.002	–	–

Table 6
Comparison between the experimental and calculated SDM for the C-101 core configuration.

SDM		
experiment [$]	T4 – ENDFB7R1 [$]	MCNP –ENDFB7R1[$]
4.83	4.75 ± 0.03	4.49 ± 0.03

Table 7
Calculated power peaking factors compared to the manufacturer data.

Factor	Manufacturer data	T4 – ENDFB7R1	MCNP –ENDFB7R1	T4/MCNP-1
f_{HR}	1.6–1.7	1.63 ± 0.01	1.62 ± 0.01	0.5% ± 0.1%
f_Z	1.2–1.3	1.28 ± 0.01	1.28 ± 0.01	0.7% ± 0.01%
f_R	1.7–1.9	1.92 ± 0.01	1.91 ± 0.01	0.3% ± 1%

ones with a relative difference of around −1.6% and −7.1% for T4 and MCNP respectively.

3.3. Power peaking factors

The power peaking factors are very important for the reactor steady-state operation, as they describe how the power density is distributed locally in every fuel element of the reactor core. These factors are considered to be the link between the neutronic and thermal hydraulic analysis of the TRIGA reactor [25]. have shown in their paper that it is very important to pay attention to power peaking factors in mixed cores, especially when performing core conversion. In this section, we present a comparison between the calculated power peaking factors and the experimental ones that are given by the manufacturer. For that reason, we calculated 3 power peaking factors:

- The hot rod power peaking factor f_{HR}: it is defined as the ratio between the fission rate (i.e. power density) in one fuel element, τ_{f_FE}, and the average fission rate in the core, τ_{f_core}. This factor is giving by the following formula:

$$f_{HR} = \frac{(\tau_{f\_FE})_{max}}{\overline{\tau_{f\_core}}} \quad \text{Eq. 5}$$

The hottest fuel element, which produces the maximum power, then corresponds to the highest f_{HR}.

- The axial power peaking factor f_Z: it describes the axial distribution of power in the fuel element. It is defined as peak-to-average fission rate $\tau_f(z)$ in the FE and it is given by the following equation:

$$f_Z = \frac{\tau_f(z)}{\overline{\tau_{fZ}}} \quad \text{Eq. 6}$$

The power peaking factor corresponds to the maximum value of f_Z.

- The radial power peaking factor f_R: it is defined as peak-to-average radial power density in the hottest FE, and it is given by the following formula:

$$f_R = \frac{\tau_f(r)}{\overline{\tau_{f_r}}} \quad \text{Eq. 7}$$

The power peaking factor corresponds to the maximum value of f_R. Figs. 6–8 illustrate the calculated power peaking factors of the TRIGA

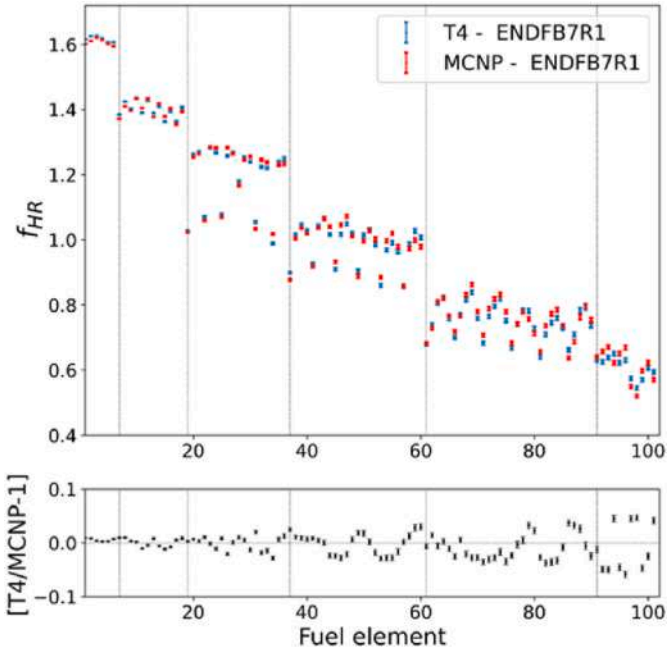

Fig. 6. Calculated f_{HR} values for all the FE of the CNESTEN's TRIGA reactor.

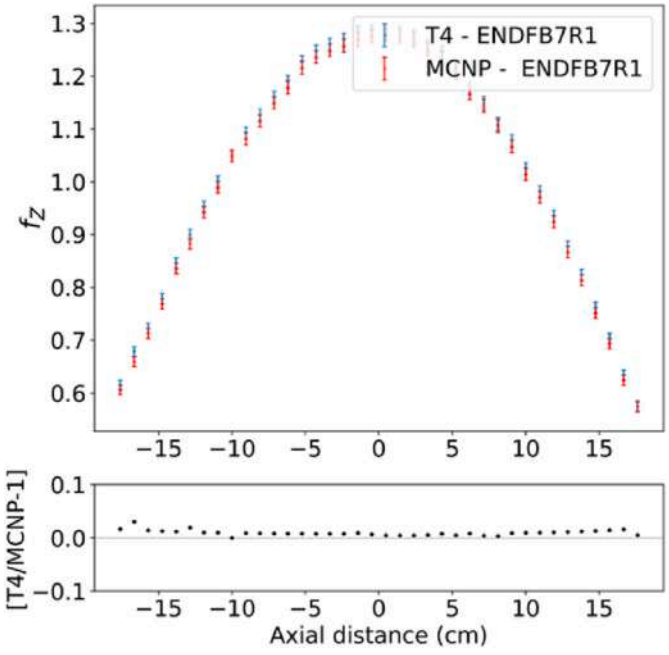

Fig. 7. Calculated axial power peaking factor f_Z for the B3, hot rod, fuel element.

reactor. It can be highlighted that:

- For the f_{HR} factor, the results show a good agreement between the calculated values. From both Figs. 6 and 9-A, one can notice that the fuel element of the B-ring undergoes the highest fission rate in the reactor core. Thus, the hottest fuel element was found to be the B3 FE located in ring B with a f_{HR} value of 1.63 and 1.62 for T4 and MCNP respectively. These values are in good agreement with the manufacturer data (cf. Table 7).
- As shown in Fig. 7, the f_Z factor, for both T4 and MCNP, reaches its maximum in the center of the fuel element, which corresponds to the maximum fission rate (i.e., maximum power density). This can also be seen clearly in Fig. 9-B which shows the relative distribution of the axial power density in the reactor core. The maximum peak-to-average value of f_Z factor for the hottest FE was found to be 1.28 with both T4 and MCNP models, which agrees with the interval provided by the manufacturer (cf. Table 7).

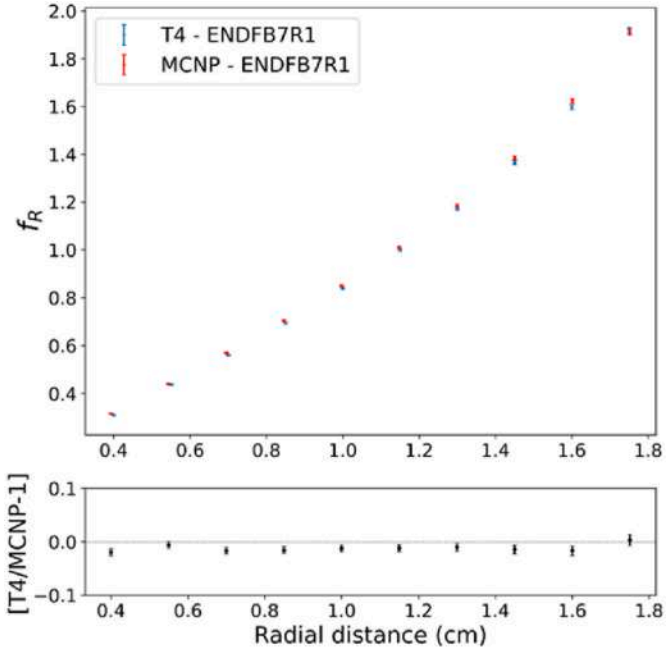

Fig. 8. Calculated radial power peaking factor f_R for the B3, hot rod, fuel element.

- As shown in Fig. 8, the f_R factor reaches a maximum value of 1.92 and 1.91, for T4 and MCNP respectively, at the external radius of the FE. These values are slightly higher than those given by the manufacturer ($1.7 < f_R < 1.9$). Moreover, the comparison shows a good agreement between the calculated values, with a relative difference lower than 0.3% ± 1%.

As reported in Table 7, the calculated power peaking factors are also in a good agreement with the manufacturer data that are available in the Final Safety Analysis Report (FSAR) of the TRIGA reactor.

3.4. Radial distributions of neutron flux

The radial neutron flux distribution was calculated in each cell (6 × 6 × 6 mm) of a rectangular virtual mesh. Fig. 10 presents the calculated T4 (ENDFB7R1) radial flux distributions in the TRIGA reactor core. The statistical uncertainty for all of these calculations varies from 0.1%, for the points closest to the core, to 4% for the most distant points. It should be mentioned that the calculated results were normalized to the maximum value in order to be compared qualitatively. Additionally, the neutron energy groups used for the calculation of each neutron flux component is based on that given by the manufacturer:

- Thermal neutron flux: 10^{-5} – 0.4 eV.
- Epithermal neutron flux: 0.4 eV–9.15 keV.
- Fast neutron flux: 9.15 keV–20 MeV.

The radial distribution of total neutron flux (cf. Fig. 10-A) in the reactor shows a maximum at the core center which corresponds to 1.30 × 10^{14} n.cm^{-2}.s^{-1} (when normalized to 2 MW). The total neutron flux decreases symmetrically as it moves away from the center towards the peripheral fuel and graphite elements (G-ring) of the reactor. The distribution of radial fast neutron flux is shown in Fig. 10-B. It can be seen

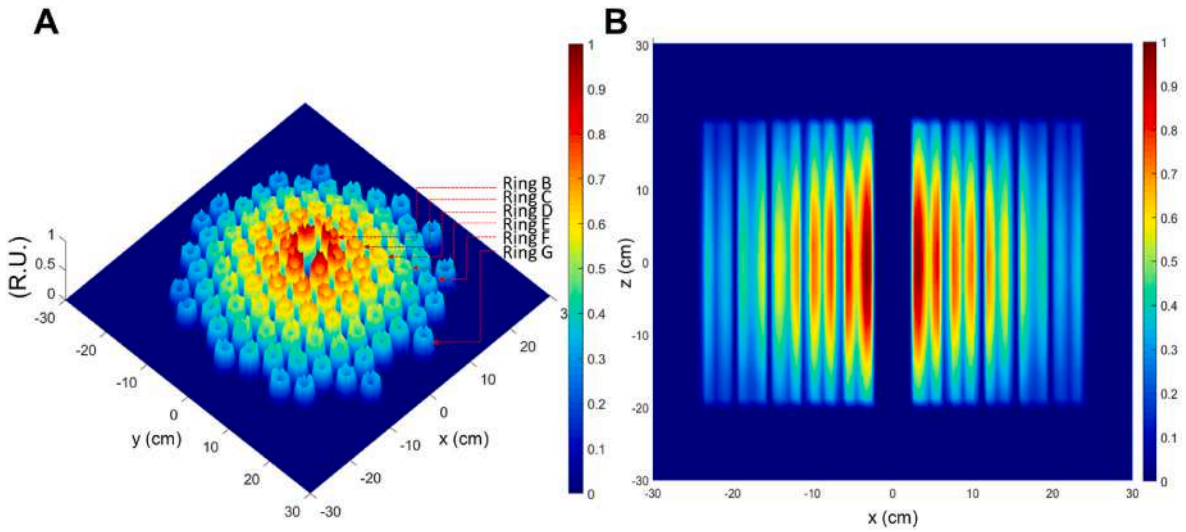

Fig. 9. (A) Relative radial and (B) axial power density distributions (relative units) in the core of TRIGA reactor.

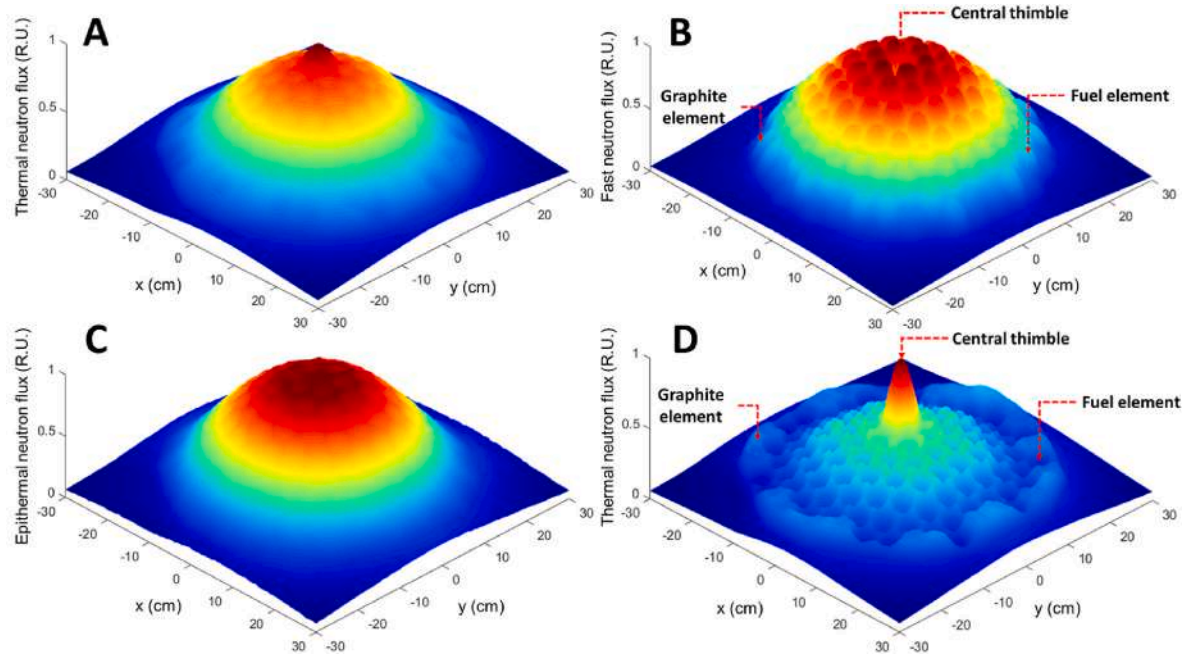

Fig. 10. Total, fast, epithermal and thermal neutron flux distributions calculated with T4.

that the fuel elements of B and C rings contribute to a large part of the fast neutron flux. These fuel elements undergo a high fission rate compared to the other fuel elements (cf. Fig. 9-A).

On the other hand, one can notice that the fast neutron flux attains its minimal value in the core center, which corresponds to the central thimble (water-filled channel). This is mainly due to the slowing down of fast fission neutrons through elastic and inelastic collisions in the water moderator. As shown in Fig. 10-D, the radial distribution of thermal neutron flux shows a peak at the core center due to the presence of the central thimble at the core center. One can notice a slight increase in the thermal flux in the G-ring, which is attributable to the graphite elements that allow to slow down fast neutrons.

Fig. 11 displays the comparison between the calculated T4 and MCNP radial neutron flux distributions in the reactor core. It is worth mentioning that the volume-averaged neutron flux is calculated using a virtual meshes that are defined in the same way by the two models in order to allow the comparison of the results. Fig. 11 shows that T4 and MCNP results are in good agreement for all the calculation points that are inside the reactor core with a relative difference around $\pm 1\% \pm 1\%$, $\pm 2\% \pm 1\%$, $\pm 2\% \pm 1\%$ and $\pm 2\% \pm 1\%$ for the total, fast, epithermal and thermal neutron flux respectively. Nevertheless, one can notice that the relative differences increase gradually when approaching the aluminum reactor core vessel and the graphite reflector. These relative differences are significant for the thermal neutron flux and are around $\pm 6\% \pm 3\%$ for the points located in the graphite.

It should be mentioned that the axial neutron flux distribution and the neutron spectra are also calculated and compared but not presented in this study to keep the article succinct.

3.5. K-eigenvalue sensitivity coefficients and uncertainty quantification

3.5.1. K-eigenvalue sensitivity coefficients

In order to assess and analyze uncertainties associated with nuclear data in the multiplication factor k_{eff}, one of the most widely used method

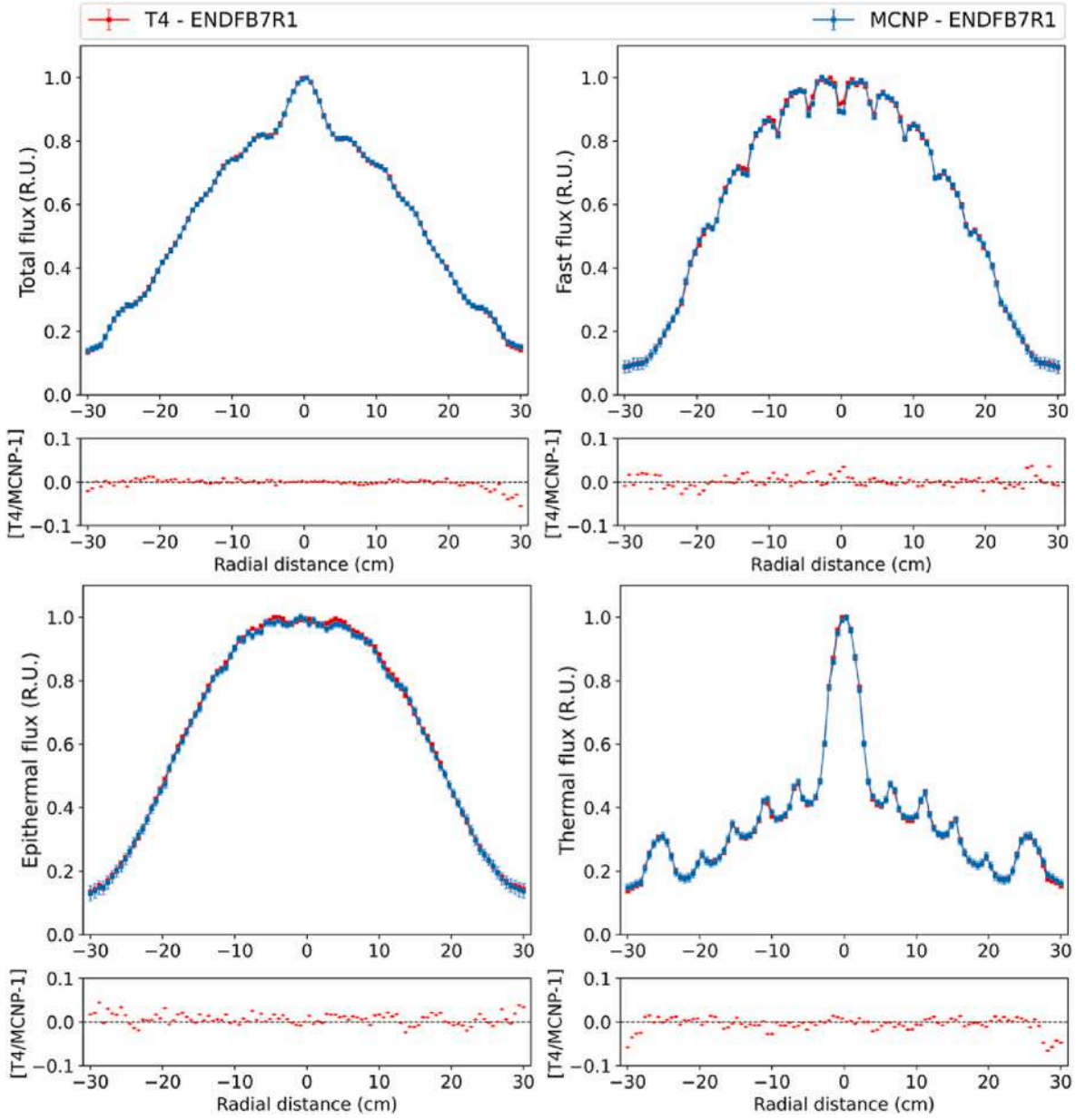

Fig. 11. Comparison between calculated T4 and MCNP radial neutron flux distributions in the reactor core.

requires the calculation of the sensitivities of this factor to nuclear data. In fact, a sensitivity coefficient expresses the variation of a reactor parameter induced by an infinitesimal variation of another parameter: it is the expression of a first order derivative. In neutronics, the sensitivity $S_{k_{eff}/\sigma_{i,r}}$ of the k_{eff} is generally expressed with respect to the cross section of the reaction "r" of an isotope "i" in percent by percent:

$$S_{k_{eff}/\sigma_{i,r}} = \left[\frac{\partial k_{eff}}{k_{eff}} \Big/ \frac{\partial \sigma_{i,r}}{\sigma_{i,r}}\right] \quad \text{Eq. 8}$$

where $\frac{\partial k_{eff}}{\partial \sigma_{i,r}}$ can be approximated by the direct calculation of the variation δk_{eff} induced by a small variation $\delta\sigma_{i,r}$ around its reference. In the latest version of T4 (4.11), the IFP-based sensitivity coefficients of the k_{eff} with respect to nuclear data can be applied to cross sections, fission neutron yields (prompt, delayed and total), fission spectra (prompt, delayed and total) and to scattering transfer functions [11]. Accordingly, the T4 computational model was used to calculate the energy-dependent sensitivity profiles of the k_{eff} using 26 energy groups optimized for water reactors [12], with a detailed description of the first resonances (cf. Table 8). The calculated sensitivity coefficients are going to be used to carry out nuclear data uncertainty quantification to the k_{eff} (cf. 4.5.2).

Table 8
26 neutron-energy groups used for sensitivity and uncertainty quantification.

Energy group	Upper energy (MeV)	Energy group	Upper energy (MeV)
1	1.9640E+01	14	1.2509E-06
2	4.9659E+00	15	1.1480E-06
3	2.2313E+00	16	1.1040E-06
4	1.3369E+00	17	1.0090E-06
5	4.9400E-01	18	9.6396E-07
6	1.9501E-01	19	8.8003E-07
7	6.7380E-02	20	6.2500E-07
8	2.4999E-02	21	3.5299E-07
9	9.1188E-03	22	2.3119E-07
10	1.9105E-03	23	1.3800E-07
11	4.1080E-04	24	7.6497E-08
12	5.2673E-05	25	3.4400E-08
13	4.0000E-06	26	1.0451E-08

Figs. 12–18 present the energy-dependent sensitivity profiles of TRIGA's k_{eff} calculated for different nuclides and reactions. For comparison purposes, the simulations were performed using the JEFF3.1.1 and ENDFB7R1 nuclear data libraries in order to identify any discrepancies in the calculation of sensitivity profiles. The comparison shows a fairly good agreement between the sensitivity profiles for the different nuclides and reactions. Only small differences were observed on the ^{235}U and ^{56}Fe elastic scattering reactions and can mainly be attributed to the differences between the two cross section libraries (JEFF3.1.1 and ENDFB7R1). Since the results are nearly identical between the two libraries, only ENDFB7R1 sensitivity profiles will be used to carry out nuclear data uncertainty analysis (cf. section 4.5.2).

As one can see from the sensitivity profiles (cf. Figs. 12–18), the k_{eff} is very sensitive to the fission and capture cross sections and to the prompt neutron fission yields and spectra of the ^{235}U, to the capture cross section of the ^{238}U, ^{1}H, ^{16}O, ^{56}Fe and ^{91}Zr and to the elastic cross section of ^{1}H and ^{16}O. Furthermore, the ^{235}U sensitivity profile (cf. Fig. 12) presents a peak for the fission, capture and total fission yield reactions. This peak occurs around the thermal energy region of the neutron spectrum (0.025 eV) which corresponds to the highest fission probability of ^{235}U.

In addition, one can also notice that the sensitivity profile of the ^{238}U capture cross section (cf. Fig. 13) shows peaks in the epithermal energy region of neutron spectrum (0.025 eV–0.4 eV) that are related to the resonances of the ^{238}U capture cross section. In fact, those peaks are due to neutron scattering reactions that allow neutrons to slow down and escape the resonance region.

The sensitivity profiles of ^{1}H, ^{16}O, ^{56}Fe and ^{12}C scattering reactions (cf. Fig. 14, 15, 16 and 17) show peaks around the fast energy domain of the neutron spectrum. For scattering reactions, those peaks occur around a neutron energy of 2 MeV which corresponds to the average energy of neutrons produced by the fission of ^{235}U. Those fast neutrons, and through collisions with the ^{1}H, ^{16}O, and ^{12}C nuclei that compose the moderator (light water) and the graphite reflector, they slow down until they reach the thermal energy (0.025 eV) to start the nuclear chain process.

The integrated sensitivity coefficients obtained by T4, By MCNP and by SCALE-6.2, using ENDFB7R1 cross section library, for the 6 main nuclei contributors to the k_{eff} sensitivity for the TRIGA reactor are shown in Table 9. The MCNP and SCALE-6.2 results, that are reported in the [26] study, were obtained by performing eigenvalue sensitivity calculations using two approaches; The IFP approach, which is applied within the MCNP/KSEN card and the Contribution-Linked eigenvalue sensitivity/Uncertainty estimation via Track-length importance Characterization (CLUTCH) approach [27,28]. The latter approach is provided in TSUNAMI-3D control sequence implemented in the SCALE package.

From Table 9, one can assume that the integrated sensitivity values calculated with T4 model are in good agreement with those calculated by MCNP and SCALE-6.2. It can be highlighted that the C-graphite (n, n) obtained by T4-IFP has a relative difference of around −8% and −6% compared to MCNP-IFP and SCALE-CLUTCH, respectively. The differences obtained can be attributed to different approaches used in T4, MCNP and SCALE-6.2 simulation codes. Besides, the MCNP and SCALE-6.2 models involve some additional details of the reactor material composition as well as some slight changes in the components nominal dimensions [26]. Further, the other integrated sensitivity values are very close between T4, MCNP and SCALE. The differences between them are smaller than 5%.

3.5.2. Nuclear data uncertainty analysis

Using the sensitivity profiles and the nuclear data covariance matrix C, the k_{eff} uncertainty due to nuclear data can be evaluated using the following formula:

$$\frac{\Delta k_{eff}}{k_{eff}} = \sqrt{S_{k_{eff}/\sigma_{i,r}} C S^{T}_{keff/\sigma_{i,r}}} \qquad \text{Eq. 9}$$

where $S_{k_{eff}/\sigma_{i,r}}$ and $S^{T}_{keff/\sigma_{i,r}}$ are the energy-dependent sensitivity profiles with T indicates transpose and C is the covariance matrix associated with neutron cross-sections. It is worth mentioning that the covariance matrices used in this study are taken from the *COvariance MAtrices of Cadarache* (COMAC-V2.1) database [12]. This database offers covariance matrices in different multi-group formats, including 26 and 36 neutron-energy groups, both derived from SHEM mesh with 281 neutron-energy groups [29], 33 neutron-energy groups for fast neutron reactor applications used in particular in the ECCO/ERANOS system [30,31] and 8 neutron-energy groups, that can be used for research and development purposes. Furthermore, this database uses differential and integral experiments in the re-estimation process of nuclear data to obtain reliable covariance matrices for the main actinides in the COMAC

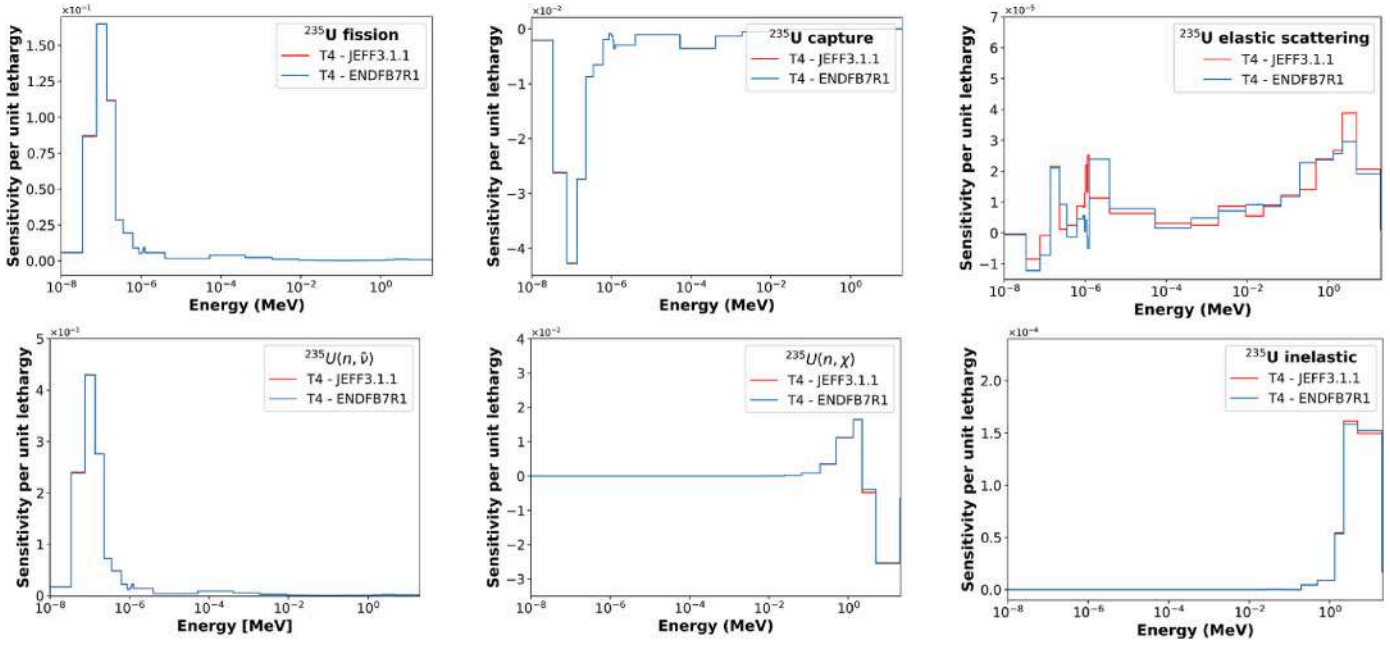

Fig. 12. Energy-dependent sensitivity profiles of TRIGA's k_{eff} calculated for multiple reactions of ^{235}U.

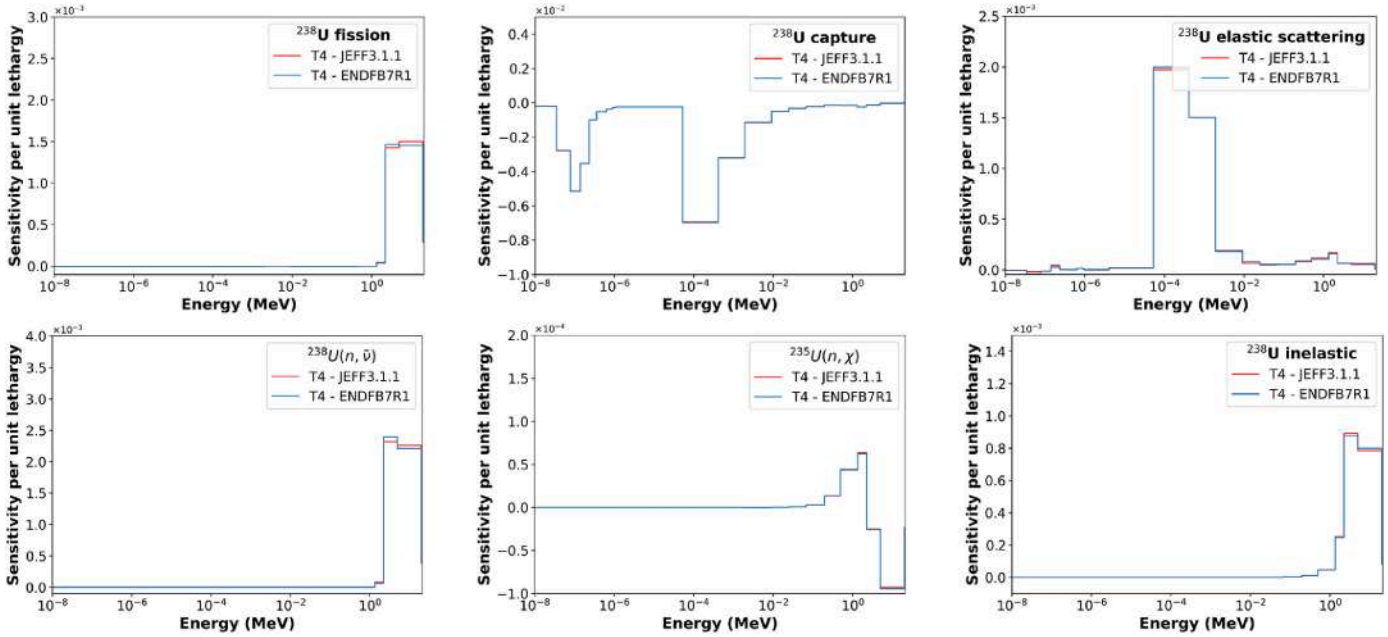

Fig. 13. Energy-dependent sensitivity profiles of TRIGA's k_{eff} calculated for multiple reactions of ^{238}U.

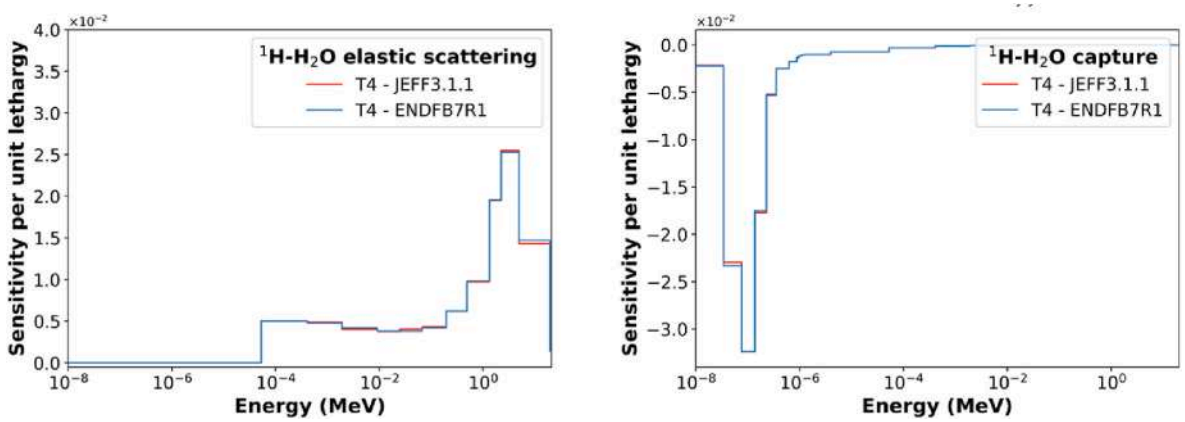

Fig. 14. Energy-dependent sensitivity profiles of TRIGA's k_{eff} calculated for elastic scattering and capture reactions of ^{1}H.

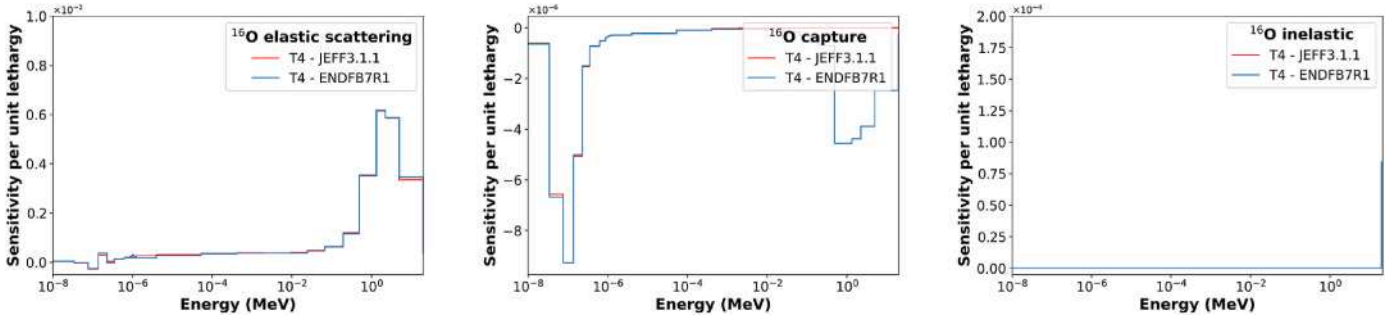

Fig. 15. Energy-dependent sensitivity profiles of TRIGA's k_{eff} calculated for elastic scattering and capture reactions of ^{16}O.

database [32,33]. In this study, the COMAC covariance matrices (cf. Annexes) are used with the same 26 neutron-energy groups that are presented in Table 8.

Table 10 presents a summary of k_{eff} nuclear data uncertainty quantification for the main nuclide-reactions associated to the material composition of the TRIGA computational model. Before digging into the comparisons, it is worth mentioning that the 44-group cross section covariance matrices of the ENDFB7R1, used in Ref. [34] study, were processed using the NJOY99 code whereas the 56-group cross section covariance matrices used in Ref. [26] study are provided with SCALE-6.2 package (56groupcov7.1). As mentioned in Ref. [35], the SCALE-6.2 covariance data has been assembled from a variety sources,

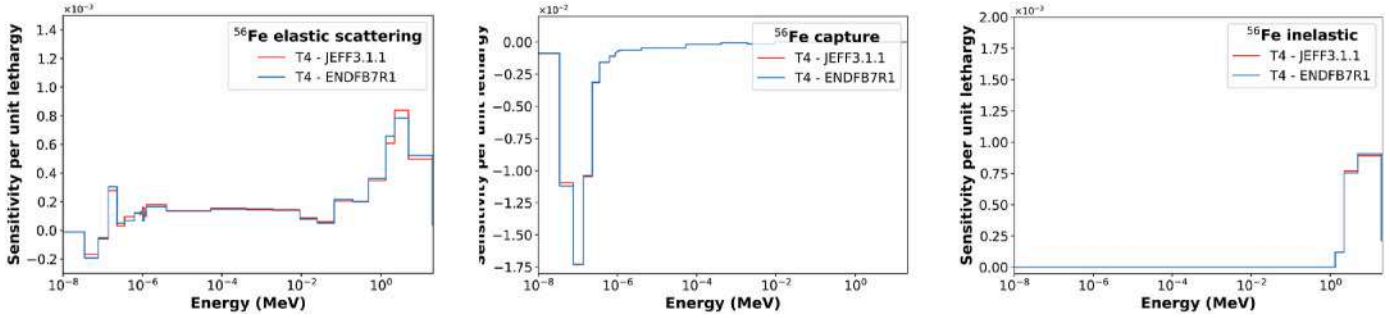

Fig. 16. Energy-dependent sensitivity profiles of TRIGA's k_{eff} calculated for elastic scattering and capture reactions of ^{56}Fe.

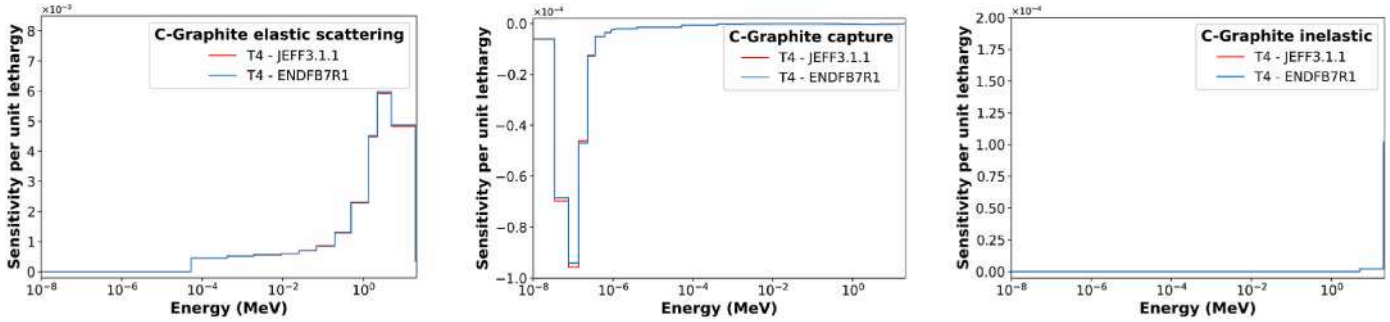

Fig. 17. Energy-dependent sensitivity profiles of TRIGA's k_{eff} calculated for elastic scattering reaction of C-graphite.

including high-fidelity covariance evaluations from ENDFB7R1, other domestic and international evaluations, as well as approximate uncertainties obtained from a collaborative project performed by Brookhaven National Laboratory, Los Alamos National Laboratory, and ORNL.

As reported in Table 10, the principal contributors to the k_{eff} nuclear data uncertainty are the ^{235}U (n,f), ^{235}U (n,γ), ^{235}U $(n,\bar{\nu})$, ^{235}U (n,χ), ^{1}H (n,γ), ^{1}H (n,n), ^{56}Fe (n,γ) and ^{91}Zr (n,γ) nuclide-reactions. It can be highlighted that:

- The k_{eff} uncertainties for ^{235}U (n,f) and ^{235}U (n,γ) are in good agreement. The differences are relatively small between COMAC-V2.1, ENDFB7R1 and SCALE-6.2.
- The k_{eff} uncertainties for both ^{235}U $(n,\bar{\nu})$ and ^{235}U (n,χ) are around 302 and 222 pcm using COMAC-V2.1 and around 378 and 353 pcm using SCALE-6.2. On the other hand, the ENDFB7R1 gives a ^{235}U $(n,\bar{\nu})$ uncertainty that is 2 times larger compared to COMAC-V2.1and SCALE-6.2. These differences are mainly due to the differences between the covariance data.
- ENDFB7R1 determines slightly larger uncertainty of 56 pcm for ^{238}U (n,γ), compared to 39 pcm and 45 pcm for COMACV-2.1 and SCALE-6.2, respectively. The ^{238}U (n,n) uncertainty is found to be consistent between COMAC-V2.1 and SCALE-6.2 whereas ENDFB7R1 determines a smaller uncertainty.
- The COMACV-2.1 uncertainty for ^{1}H (n,n) shows a relatively good agreement with SCALE-6.2 with a relative difference of 2% and 0.4%, respectively. On the other hand, the ^{1}H (n,γ) uncertainty is consistent between COMAC-V2.1 and SCLAE-6.2 with a relative difference of 15%. Furthermore, the ENDFB7R1 overestimates the ^{1}H (n,n) and ^{1}H (n,γ) uncertainties by a factor of 2 compared to the other libraries.
- The uncertainty related to ^{16}O (n,n) is around 30 pcm for COMACV-2.1, ENDFB7R1 and around 40 pcm for the SCALE-6.2. Given that the ^{16}O (n,n) integrated sensitivity has a relative difference of −1.3% between T4 and SCALE-CLUTCH (cf. Table 9), the difference in the uncertainty can be due to a high ^{16}O (n,n) cross section uncertainty in the SCALE-6.2 covariance data.
- A large difference is observed between COMACV-2.1 and SCALE-6.2 uncertainty estimation for ^{56}Fe (n,γ). Once again, this difference can be attributed to the differences in the covariance data since the integrated sensitivity values calculated by T4 and SCALE-6.2 are almost identical.
- The uncertainties for ^{91}Zr (n,γ), ^{91}Zr (n,n) and ^{91}Zr (n,n') are in good agreement between the COMAC-V2.1 and SCALE-6.2, only small discrepancies are observed.
- This work shows that the ^{92}Zr (n,γ) reaction has a large uncertainty of 186 pcm which contributes by 10% to the total k_{eff} nuclear data uncertainty. One can also note that the uncertainties related of the capture, elastic and inelastic scattering reactions of the ^{90}Zr, ^{92}Zr, and ^{94}Zr are not negligible and should be taken into account while performing k_{eff} nuclear data uncertainty quantification.

To sum up, the total nuclear data uncertainty (1σ) in the k_{eff} ranges between 585 pcm for T4 - COMAC-V2.1, 708 pcm for SCALE-6.2 (56groupcov7.1) and 946 for MCNP (ENDFB7R1).

4. Conclusion

This study sums up the development and the validation of the new detailed T4 computational model of the CNESTEN's TRIGA Mark II research reactor and the sensitivity analysis and nuclear data uncertainty quantification. Different comparisons with the reference MCNP model, for various core configurations, were performed in order to prove the consistency and the reliability of this new model. Through these comparisons, we have demonstrated that the T4 model is able to reproduce the calculated MCNP and the experimental results obtained during the qualification phase of the reactor. Only small discrepancies were observed on the calculation of the kinetic parameters of the reactor with a maximum difference (with regards to MCNP – ENDFB7R1) of around 144 pcm, −1% and 4.5% for k_{eff}, β_{eff} and Λ respectively. Furthermore, the core excess reactivity was determined for the current

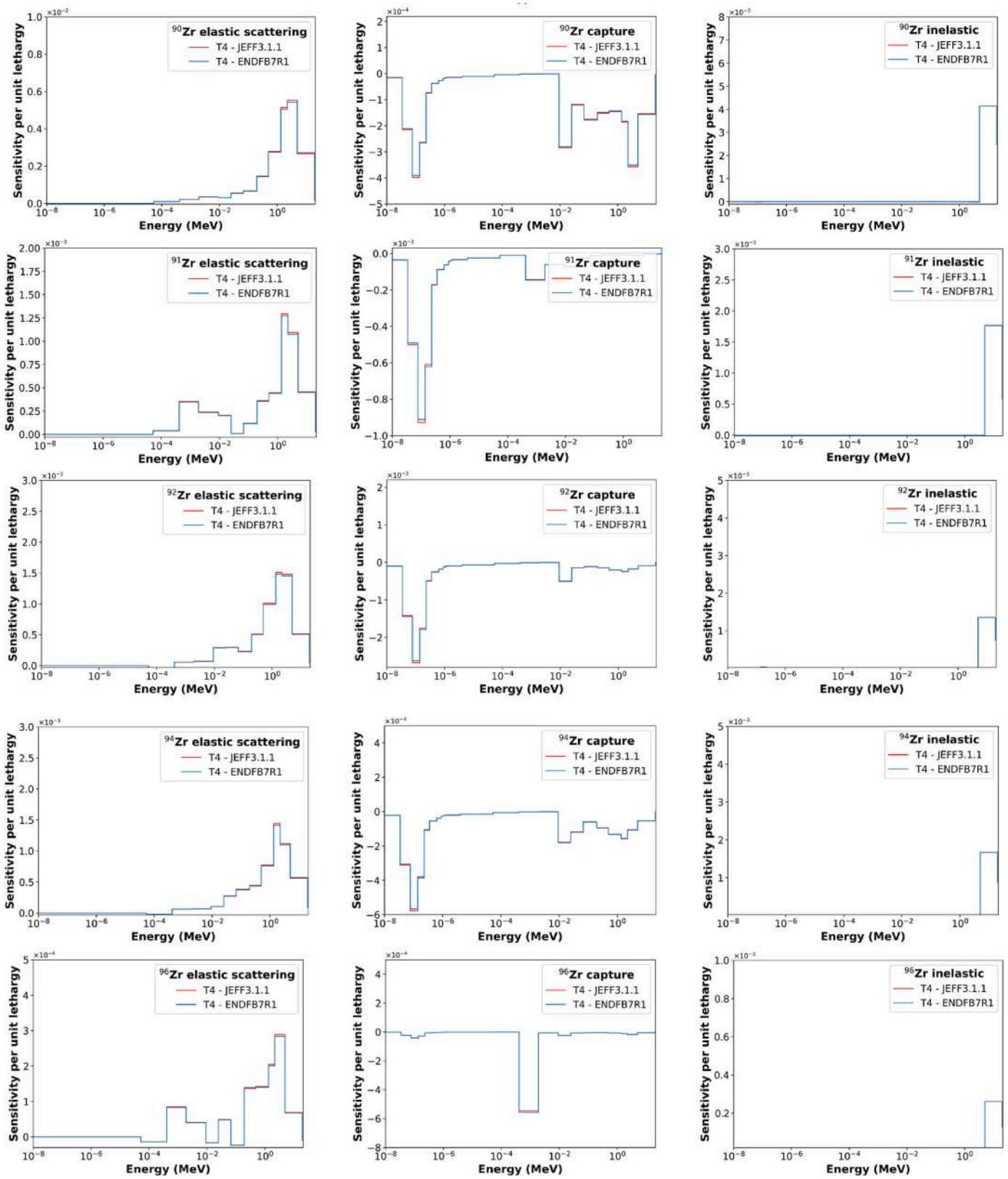

Fig. 18. Energy-dependent sensitivity profiles of TRIGA's k_{eff} calculated for elastic scattering, capture and inelastic scattering reactions of ^{90}Zr, ^{91}Zr, ^{92}Zr, ^{94}Zr and ^{96}Zr, respectively.

Table 9
Energy integrated sensitivity coefficients and comparisons with results obtained with other simulation codes (nuclear data library ENDFBVIIR1).

Nuclide-reaction	T4 – IFP	u3 (%)	MCNP – IFP	U[a] (%)	SCALE-6.2 – CLUTCH	u^2 (%)
$^{235}U\ (n,f)$	3.83E-01	0.01	3.83E-01	0.06	3.83E-01	0.01%
$^{235}U\ (n,\bar{\nu})$	9.96E-01	0.01	9.96E-01	0.02	9.96E-01	0.01
$^{235}U\ (n,\chi)$	0.00E-00	0.00	0	0	0	0
$^{238}U\ (n,n)$	4.41E-03	0.66	4.34E-03	2.31	4.33E-03	0.50
$^{238}U\ (n,\gamma)$	−4.01E-02	0.02	−3.98E-02	0.07	−3.98E-02	0.01
$^{238}U\ (n,\bar{\nu})$	3.62E-03	0.11	–	–	–	–
$^{1}H\ (n,n)$	2.65E-01	0.30	2.73E-01	0.92	2.73E-01	0.66
$^{16}O\ (n,n)$	2.19E-02	0.37	2.23E-02	1.26	2.22E-02	0.37
$^{56}Fe\ (n,\gamma)$	−4.23E-02	0.01	−4.21E-02	0.02	−4.19E-02	0.01
$^{91}Zr\ (n,n)$	4.64E-03	1.23	4.89E-03	3.88	4.82E-03	0.88
$^{91}Zr\ (n,\gamma)$	−2.65E-02	0.07	−2.75E-02	0.03	−2.66E-02	0.01
C-gra (n,n)	2.39E-02	1.41	2.58E-02	0.99	2.54E-02	0.42

[a] u: refers to the relative 1σ statistical uncertainty given in %.

Table 10
k_{eff} nuclear data uncertainty quantification for the TRIGA reactor and comparisons with results obtained with various simulation codes and nuclear data libraries.

Isotope and reaction	$\Delta k_{eff}/k_{eff}$ (pcm)		
	T4 + COMAC-V2.1	MCNP + ENDFB7R1 [34]	SCALE-6.2 + 56groupcov7.1 [26]
$^{235}U\ (n,f)$	**132**	**132**	**131**
$^{235}U\ (n,n)$	0.37	3	1
$^{235}U\ (n,\gamma)$	**167**	**166**	**165**
$^{235}U\ (n,\bar{\nu})$	**302**	**688**	**378**
$^{235}U\ (n,\chi)$	**222**	**394**	**353**
$^{235}U\ (n,n')$	2	2	2
$^{238}U\ (n,f)$	6	1	1
$^{238}U\ (n,n)$	14	4	14
$^{238}U\ (n,\gamma)$	**39**	**56**	**45**
$^{238}U\ (n,\bar{\nu})$	2	5	4
$^{238}U\ (n,\chi)$	1	2	3
$^{238}U\ (n,n')$	**10**	**30**	**26**
$^{1}H\ (n,\gamma)$	**200**	**411**	**173**
$^{1}H\ (n,n)$	**102**	**218**	**102**
$^{16}O\ (n,\gamma)$	1	1	1
$^{16}O\ (n,n)$	**31**	**29**	**40**
$^{16}O\ (n,n')$	1	–	1
$^{56}Fe\ (n,\gamma)$	**121**	–	**235**
$^{56}Fe\ (n,n)$	9	–	11
$^{56}Fe\ (n,n')$	4	–	7
$^{90}Zr\ (n,n)$	**67**	–	–
$^{90}Zr\ (n,\gamma)$	**29**	–	–
$^{90}Zr\ (n,n')$	37	–	–
$^{91}Zr\ (n,n)$	16	–	16
$^{91}Zr\ (n,\gamma)$	**209**	-	**204.8**
$^{91}Zr\ (n,n')$	**22**	-	**22**
$^{92}Zr\ (n,n)$	29	–	–
$^{92}Zr\ (n,\gamma)$	**186**	–	–
$^{92}Zr\ (n,n')$	**12**	–	–
$^{94}Zr\ (n,n)$	**30**	–	–
$^{94}Zr\ (n,\gamma)$	7	–	–
$^{94}Zr\ (n,n')$	17	–	–
$^{96}Zr\ (n,n)$	6	–	–
$^{96}Zr\ (n,\gamma)$	5	–	–
$^{96}Zr\ (n,n')$	3	–	–
C-gra (n,n)	13	–	14
C-gra (n,γ)	1	–	1
C-gra (n,n')	3	–	3
Total (pcm)	**585**	**946**	**708**

core operating configuration and the calculated values are consistent with experimental ones. The control rods worth is also calculated and compared with the experimental values and a reasonably good agreement was observed among all the FFCR. However, both models slightly underestimate the experimental values for the SHIM IV and RGULATING control rods. Additionally, both T4 and MCNP models have proven their accuracy to calculate the power peaking factors and the radial flux distributions.

Sensitivity analysis and nuclear data quantification were also carried out in this study. For this purpose, the T4 computational model was used to calculate the sensitivity profiles for different nuclides/reactions that are associated to the material data of the TRIGA reactor. The results show that the energy-dependent sensitivity profiles derived from the ENDFB7R1 and JEFF3.1.1 nuclear data libraries are almost identical except for the C-graphite. The nuclear data uncertainty was then quantified based on the COMAC-V2.1 covariance matrices and the sensitivity profiles. The principal contributors to the k_{eff} nuclear data uncertainty were found to be the $^{235}U\ (n,f)$ with 5%, $^{235}U\ (n,\gamma)$ with 8%, $^{235}U\ (n,\bar{\nu})$ with 27%, $^{235}U\ (n,\chi)$ with 14%, $^{1}H\ (n,\gamma)$ with 12%, $^{1}H\ (n,n)$ with 3%, $^{56}Fe\ (n,\gamma)$ with 4%, $^{91}Zr\ (n,\gamma)$ with 13% and $^{92}Zr\ (n,\gamma)$ with 10% to the total k_{eff} uncertainty. This study also shows that the contribution of zirconium (in UZrH) to the total uncertainty is not negligible and that it should be taken into account when performing S/U analysis for TRIGA types of the reactor. From the comparisons with previous S/U studies, we can conclude that the differences are, for some nuclide-reactions, significant and that might be principally due to the differences between the covariance matrices' databases: COMAC-V2.1, ENDFB7R1, JENDL-4.0 and SCALE-6.2. All things considered; it seems reasonable to assert that further efforts are needed to evaluate high fidelity nuclear covariance data allowing for the achievement of reliable nuclear data uncertainties.

It is worth-mentioning that further work is ongoing so as to extend the experimental validation of these computational models. The collaboration between the CEA and the CNESTEN should make it possible to expand the utilization of the TRIGA computational models by carrying out new experiments, allowing an advanced neutron and photon characterization of the irradiation facilities of the reactor. In fact, an experimental campaign was carried out in the CNESTEN's TRIGA reactor in order to accurately characterize the neutron and photon flux in different irradiation channels of the reactor, by combining different nuclear measurement methods and techniques. The results of these measurement are currently being analyzed.

Declaration of competing interest

The authors declare that they have no known competing financial interests or personal relationships that could have appeared to influence the work reported in this paper.

Acknowledgements

The authors would like to thank RIZZO Axel and BELLANGER-VILLARD Véronique of the Physics Studies Laboratory (LEPh), The French Alternative Energies and Atomic Energy Commission (CEA), Saint-Paul-lez-Durance, France, for providing the COMAC-V2.1 nuclear covariance matrices database that used to carry on the uncertainty quantification in the k_{eff}.

Annexes

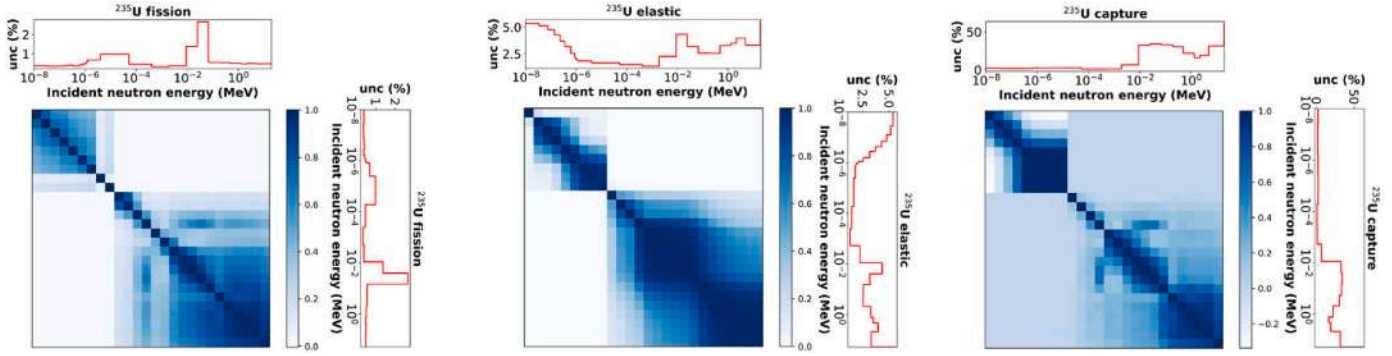

Fig. 19. ^{235}U fission, elastic and capture cross section uncertainties and energy correlations provided by COMAC-V2.1.

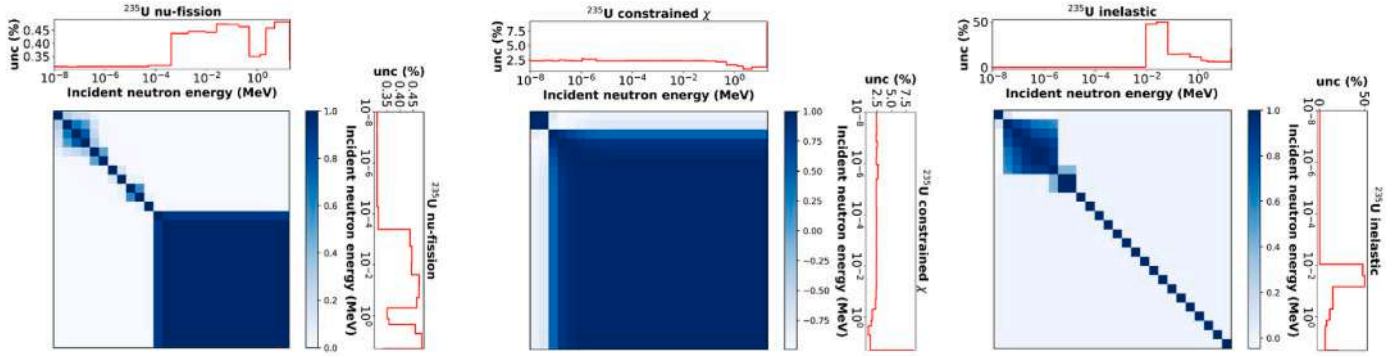

Fig. 20. ^{235}U nu-fission, constrained χ and inelastic cross section uncertainties and energy correlations provided by COMAC-V2.1.

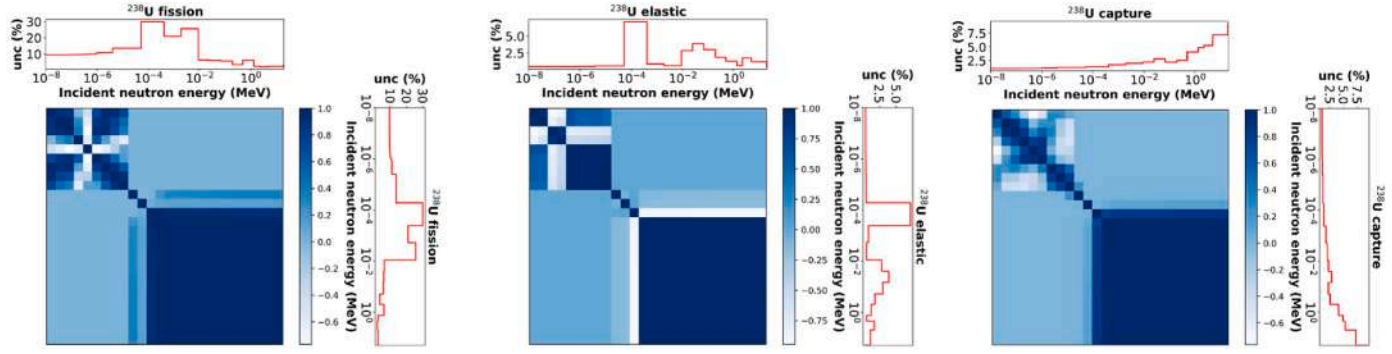

Fig. 21. ^{238}U fission, elastic and capture cross section uncertainties and energy correlations provided by COMAC-V2.1.

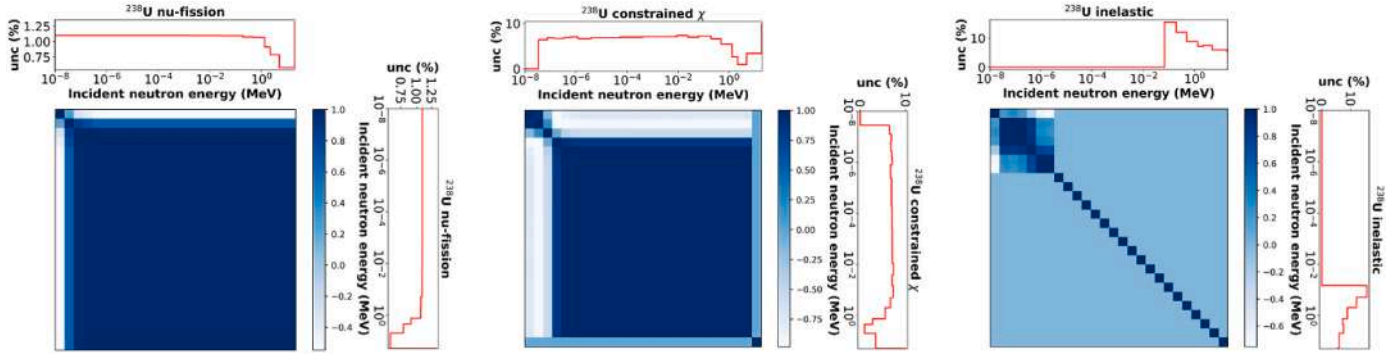

Fig. 22. 238U nu-fission, constrained χ and inelastic cross section uncertainties and energy correlations provided by COMAC-V2.1.

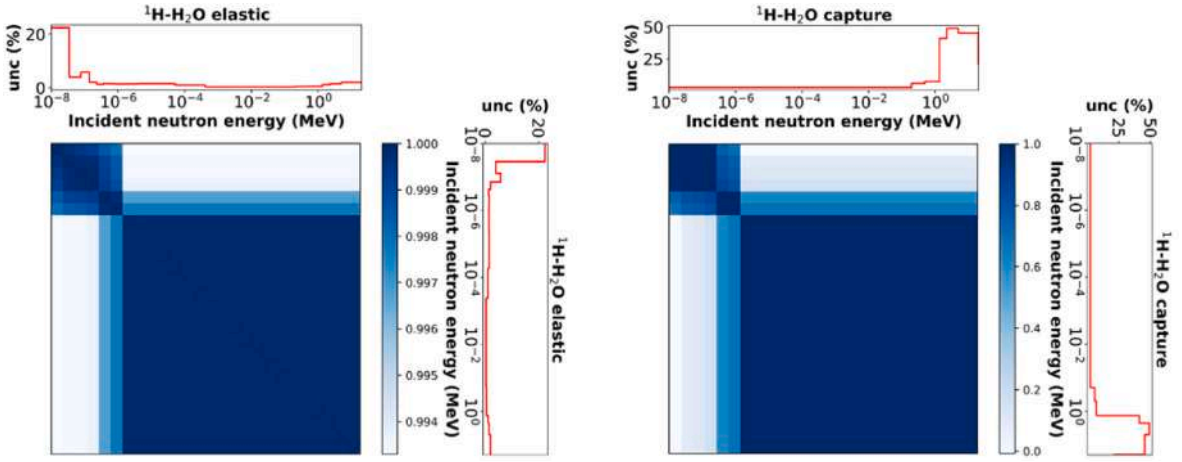

Fig. 23. 1H–H2O elastic and capture cross section uncertainties and energy correlations provided by COMAC-V2.1.

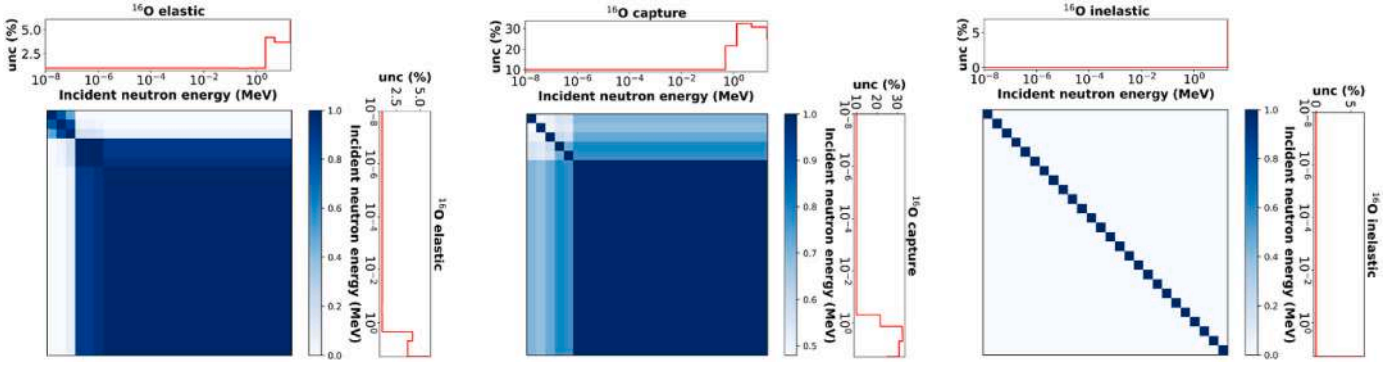

Fig. 24. 16O elastic, capture and inelastic cross section uncertainties and energy correlations provided by COMAC-V2.1.

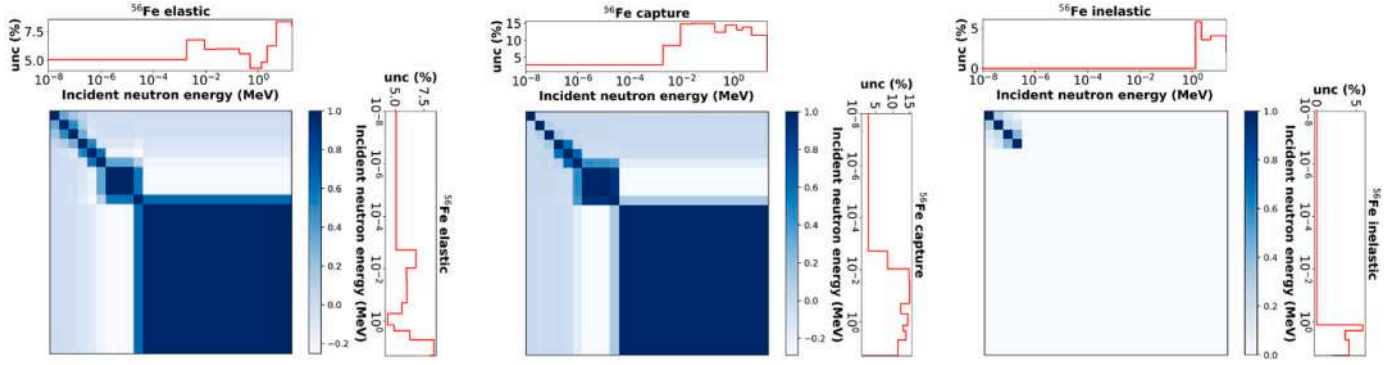

Fig. 25. 56Fe elastic, capture and inelastic cross section uncertainties and energy correlations provided by COMAC-V2.1.

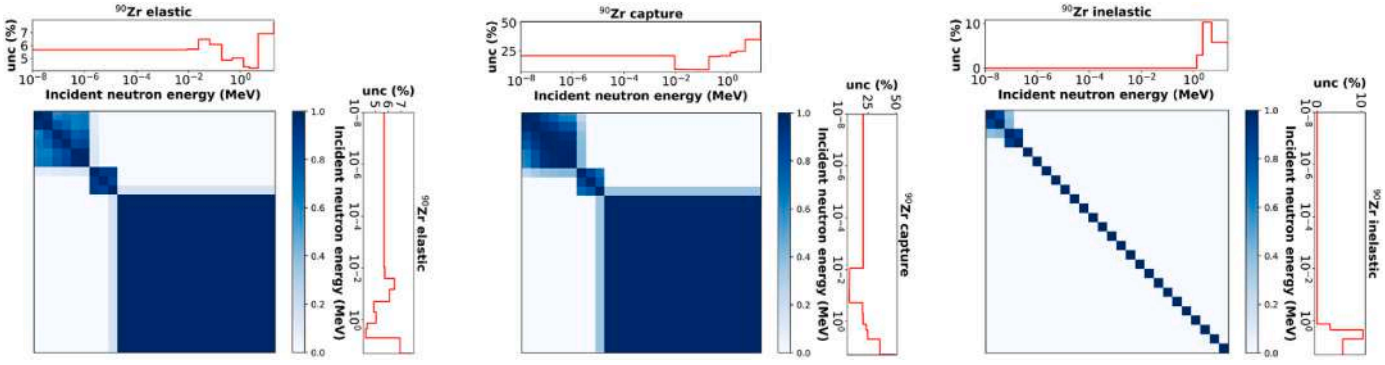

Fig. 26. 90Zr elastic, capture and inelastic cross section uncertainties and energy correlations provided by COMAC-V2.1.

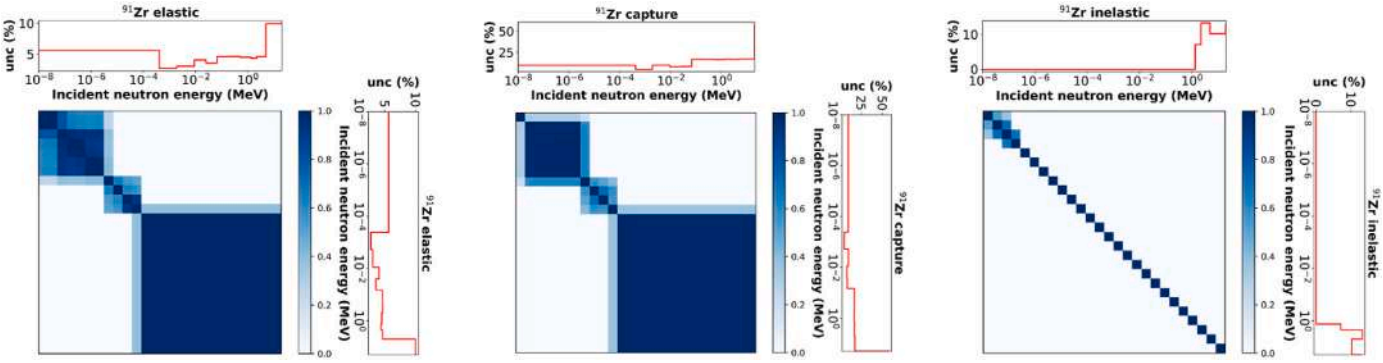

Fig. 27. 91Zr elastic, capture and inelastic cross section uncertainties and energy correlations provided by COMAC-V2.1.

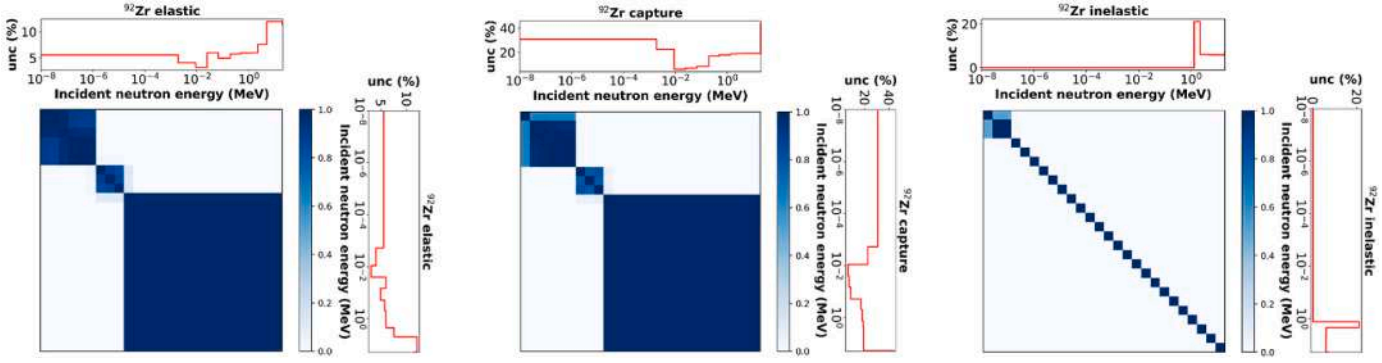

Fig. 28. 92Zr elastic, capture and inelastic cross section uncertainties and energy correlations provided by COMAC-V2.1.

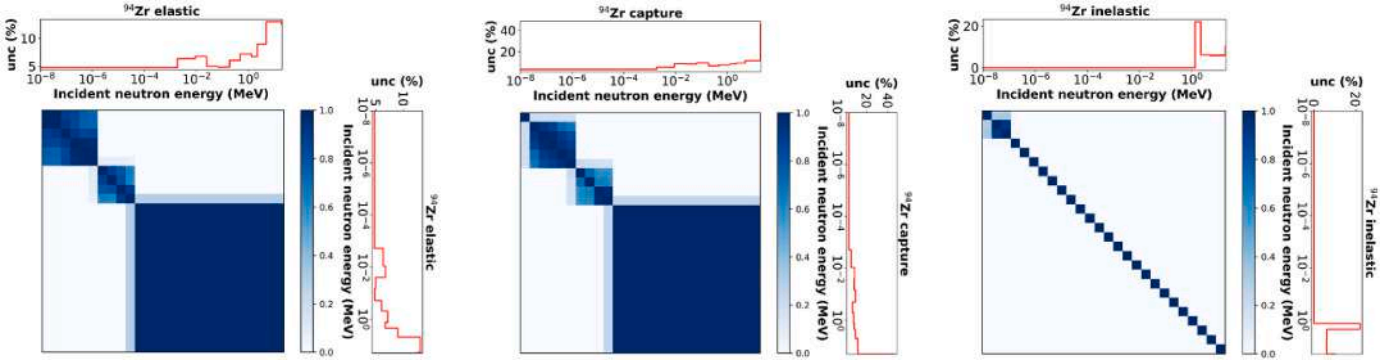

Fig. 29. 94Zr elastic, capture and inelastic cross section uncertainties and energy correlations provided by COMAC-V2.1.

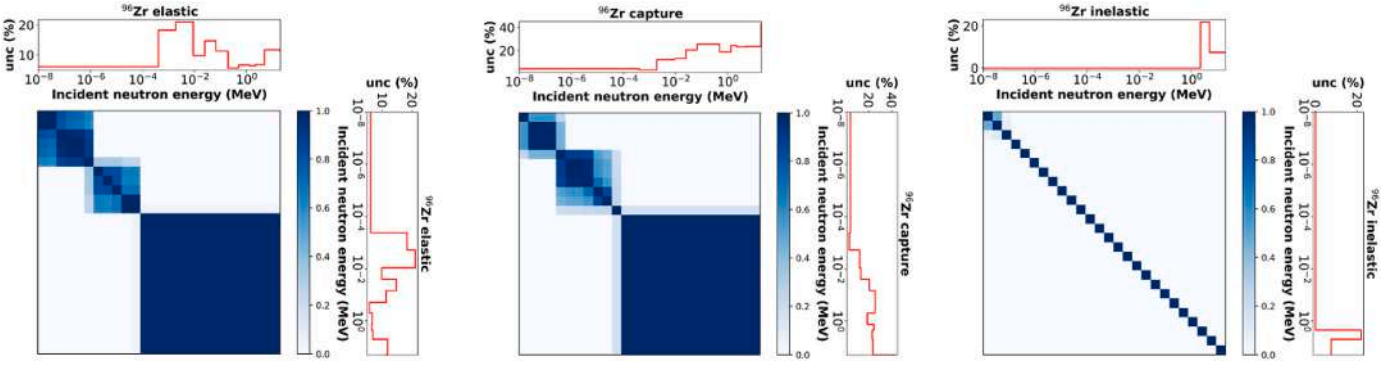

Fig. 30. ^{96}Zr elastic, capture and inelastic cross section uncertainties and energy correlations provided by COMAC-V2.1.

References

[1] A.E. Craft, B.A. Hilton, G.C. Papaioannou, Characterization of a neutron beam following reconfiguration of the neutron Radiography reactor (NRAD) core and addition of new fuel elements, Nucl. Eng. Technol. 48 (2016) 200–210, https://doi.org/10.1016/j.net.2015.10.006.

[2] S.W. Morgan, J.C. King, C.L. Pope, Beam characterization at the neutron Radiography reactor, Nucl. Eng. Des. 265 (2013) 639–653, https://doi.org/10.1016/j.nucengdes.2013.08.059.

[3] V. Radulović, Y. Yamazaki, Ž. Pastuović, A. Sarbutt, K. Ambrožič, R. Bernat, Z. Ereš, J. Coutinho, T. Ohshima, I. Capan, L. Snoj, Silicon carbide neutron detector testing at the JSI TRIGA reactor for enhanced border and port security, Nucl. Instrum. Methods Phys. Res. Sect. Accel. Spectrom. Detect. Assoc. Equip. 972 (2020), 164122, https://doi.org/10.1016/j.nima.2020.164122.

[4] A. Gruel, K. Ambrožič, C. Destouches, V. Radulović, A. Sardet, L. Snoj, Gamma-heating and gamma flux measurements in the JSI TRIGA reactor: results and prospects, IEEE Trans. Nucl. Sci. 67 (2020) 559–567, https://doi.org/10.1109/TNS.2020.2974968.

[5] B. El Bakkari, B. Nacir, T. El Bardouni, C. El Younoussi, Y. Boulaich, H. Boukhal, Feasibility analysis of I-131 production in the Moroccan TRIGA research reactor, Ann. Nucl. Energy 78 (2015) 140–145, https://doi.org/10.1016/j.anucene.2014.11.044.

[6] M.Q. Huda, M.S. Islam, M.M. Rahman, A. Haque, M. Uddin, Studies on the overall safety aspects during irradiation of TeO2 in the central thimble of the TRIGA research reactor, Ann. Nucl. Energy 36 (2009) 199–212, https://doi.org/10.1016/j.anucene.2008.11.013.

[7] B. El Bakkari, B. Nacir, T. El Bardouni, C. El Younoussi, O. Merroun, A. Htet, Y. Boulaich, M. Zoubair, H. Boukhal, M. Chakir, Monte Carlo modelling of TRIGA research reactor, Radiat. Phys. Chem. 79 (2010) 1022–1030, https://doi.org/10.1016/j.radphyschem.2010.04.016.

[8] B. El Bakkari, T. El Bardouni, O. Merroun, Ch. El Younoussi, Y. Boulaich, E. Chakir, Development of an MCNP-tally based burnup code and validation through PWR benchmark exercises, Ann. Nucl. Energy 36 (2009) 626–633, https://doi.org/10.1016/j.anucene.2008.12.025.

[9] B. El Bakkari, T. El Bardouni, B. Nacir, C. El Younoussi, Y. Boulaich, H. Boukhal, M. Zoubair, Fuel burnup analysis for the Moroccan TRIGA research reactor, Ann. Nucl. Energy 51 (2013) 112–119, https://doi.org/10.1016/j.anucene.2012.07.030.

[10] H. Ghninou, A. Gruel, A. Lyoussi, C. Reynard-Carette, C. El Younoussi, B. El Bakkari, B. Nacir, Y. Boulaich, H. Bounouira, Characterization of neutron reaction rates in different irradiation channels of the CNESTEN's TRIGA mark II research reactor, IEEE Trans. Nucl. Sci. 69 (2022) 1806–1814, https://doi.org/10.1109/TNS.2022.3174673.

[11] E. Brun, F. Damian, C.M. Diop, E. Dumonteil, F.X. Hugot, C. Jouanne, Y.K. Lee, F. Malvagi, A. Mazzolo, O. Petit, J.C. Trama, T. Visonneau, A. Zoia, TRIPOLI-4®, CEA, EDF and AREVA reference Monte Carlo code, Joint International Conference on Supercomputing in Nuclear Applications and Monte Carlo 2013, SNA + MC 2013. Pluri- and Trans-disciplinarity, Towards New Modeling and Numerical Simulation Paradigms, Ann. Nucl. Energy 82 (2015) 151–160, https://doi.org/10.1016/j.anucene.2014.07.053.

[12] P. Archier, C. De Saint Jean, G. Noguère, O. Litaize, P. Leconte, C. Bouret, COMAC: nuclear data covariance matrices library for reactor applications. PHYSOR - role React, Phys. Sustain. Future (2014).

[13] M.B. Chadwick, M. Herman, P. Obložinský, M.E. Dunn, Y. Danon, A.C. Kahler, D. L. Smith, B. Pritychenko, G. Arbanas, R. Arcilla, R. Brewer, D.A. Brown, R. Capote, A.D. Carlson, Y.S. Cho, H. Derrien, K. Guber, G.M. Hale, S. Hoblit, S. Holloway, T. D. Johnson, T. Kawano, B.C. Kiedrowski, H. Kim, S. Kunieda, N.M. Larson, L. Leal, J.P. Lestone, R.C. Little, E.A. McCutchan, R.E. MacFarlane, M. MacInnes, C. M. Mattoon, R.D. McKnight, S.F. Mughabghab, G.P.A. Nobre, G. Palmiotti, A. Palumbo, M.T. Pigni, V.G. Pronyaev, R.O. Sayer, A.A. Sonzogni, N.C. Summers, P. Talou, I.J. Thompson, A. Trkov, R.L. Vogt, S.C. van der Marck, A. Wallner, M. C. White, D. Wiarda, P.G. Young, ENDF/B-VII.1 nuclear data for science and technology: cross sections, covariances, fission product yields and decay data, Nucl. Data Sheets 112 (2011) 2887–2996, https://doi.org/10.1016/j.nds.2011.11.002. Special Issue on ENDF/B-VII.1 Library.

[14] A. Santamarina, D. Bernard, The JEFF-3.1.1 Nuclear Data Library, 2009. JEFF Report 22.

[15] J.C. Sublet, P. Ribon, M. Coste-Delclaux, CALENDF-2010: User Manual, 2011. Rapport CEA-R-6277.

[16] L. Snoj, A. Kavčič, G. Žerovnik, M. Ravnik, Calculation of kinetic parameters for mixed TRIGA cores with Monte Carlo, Ann. Nucl. Energy 37 (2010) 223–229, https://doi.org/10.1016/j.anucene.2009.10.020.

[17] Y. Nauchi, T. Kameyama, Development of calculation technique for iterated fission probability and reactor kinetic parameters using continuous-energy Monte Carlo method, J. Nucl. Sci. Technol. 47 (2010) 977–990, https://doi.org/10.1080/18811248.2010.9711662.

[18] G. Truchet, P. Leconte, A. Santamarina, E. Brun, F. Damian, A. Zoia, Computing adjoint-weighted kinetics parameters in tripoli-4® by the iterated fission probability method, Ann. Nucl. Energy 85 (2015) 17–26, https://doi.org/10.1016/j.anucene.2015.04.025.

[19] C. Brian Kiedrowski, Theory, Interface, Verification, Validation, and Performance of the Adjoint-Weighted Point Reactor Kinetics Parameter Calculations in MCNP. Los Alamos Natl. Lab. XCP-3 Monte Carlo Codes -UR-10-01700, 2010.

[20] Y. Nauchi, T. Kameyama, Proposal of direct calculation of kinetic parameters βeff and based on continuous energy Monte Carlo method, J. Nucl. Sci. Technol. 42 (2005) 503–514, https://doi.org/10.1080/18811248.2004.9726417.

[21] M.M. Bretscher, Evaluation of Reactor Kinetic Parameters without the Need for Perturbation Codes, 1997.

[22] M.Q. Huda, M. Rahman, M.M. Sarker, S.I. Bhuiyan, Benchmark analysis of the TRIGA MARK II research reactor using Monte Carlo techniques, Ann. Nucl. Energy 31 (2004) 1299–1313, https://doi.org/10.1016/j.anucene.2004.02.005.

[23] T. Matsumoto, N. Hayakawa, Benchmark analysis of triga mark ii reactivity experiment using a continuous energy Monte Carlo code mcnp, J. Nucl. Sci. Technol. 37 (2000) 1082–1087, https://doi.org/10.1080/18811248.2000.9714995.

[24] H. Rehman, S.-I. Ahmad, Neutronics analysis of TRIGA Mark II research reactor, Nucl. Eng. Technol. 50 (2018) 35–42, https://doi.org/10.1016/j.net.2017.11.003.

[25] L. Snoj, M. Ravnik, Power peakings in mixed TRIGA cores, Nucl. Eng. Des. 238 (2008) 2473–2479, https://doi.org/10.1016/j.nucengdes.2008.02.005.

[26] H. Ziani, T. El Bardouni, M. Lahdour, M. El Barbari, H. El Yaakoubi, Y. Boulaich, Eigenvalue sensitivity and nuclear data uncertainty analysis for the Moroccan TRIGA Mark II research reactor using SCALE6.2 and MCNP6.2, Nucl. Eng. Des. 378 (2021), 111160, https://doi.org/10.1016/j.nucengdes.2021.111160.

[27] C.M. Perfetti, B.T. Rearden, W.R. Martin, SCALE continuous-energy eigenvalue sensitivity coefficient calculations, Nucl. Sci. Eng. 182 (2016) 332–353, https://doi.org/10.13182/NSE15-12.

[28] Y. Qiu, D. She, X. Tang, K. Wang, J. Liang, Computing eigenvalue sensitivity coefficients to nuclear data based on the CLUTCH method with RMC code, Ann. Nucl. Energy 88 (2016) 237–251, https://doi.org/10.1016/j.anucene.2015.11.007.

[29] N. Hfaiedh, A. Santamarina, Determination of the optimized SHEM mesh for neutron transport calculations, M C 2005 Int. Top. Meet. Math. Comput. Supercomput. React. Phys. Nucl. Biol. Appl. (2005).

[30] G. Rimpault, D. Plisson, J. Tommasi, R. Jacqmin, J.-M. Rieunier, D. Verrier, D. Biron, The ERANOS Code and Data System for Fast Reactor Neutronic Analyses 15, 2002.

[31] G. Rimplaut, Algorithmic features of the ECCO Cell Code for treating heterogeneous fast reactor subassemblies, in: Proc. Int. Conf. Math. Comput. React. Phys. Environ. Anal., 1995.

[32] C. De Saint Jean, P. Archier, E. Privas, G. Noguère, O. Litaize, P. Leconte, Evaluation of Cross Section Uncertainties Using Physical Constraints: Focus on Integral Experiments. Nucl. Data Sheets, Special Issue on International Workshop on Nuclear Data Covariances, April 28 - May 1, 2014, Santa Fe, New Mexico, USA, 2015, pp. 178–184, https://doi.org/10.1016/j.nds.2014.12.031. t2.lanl.gov/cw2014 123.

[33] A. Santamarina, D. Bernard, Re-estimation of nuclear data and reliable covariances using integral experiments. application to jeff3 library, in: MandC2017 - International Conference on Mathematics and Computational Methods Applied to Nuclear Science and Engineering. MandC2017 - International Conference on Mathematics and Computational Methods Applied to Nuclear Science and Engineering, 2017 (Jeju, South Korea).

[34] M. Makhloul, H. Boukhal, E. Chakir, T. El Bardouni, M. Lahdour, M. Kaddour, A. Ahmed, A. Arectout, H. El Yaakoubi, Sensitivity and uncertainty quantification of neutronic integral data in the TRIGA Mark II research reactor, Nucl. Eng. Technol. 54 (2022) 523–531, https://doi.org/10.1016/j.net.2021.08.003.

[35] B.T. Rearden, M.A. Jessee, SCALE Code System, 2016. ORNLTM-200539 Version 62.

[40] X-5 Monte Carlo Team, MCNP – A General Monte Carlo N-Particle Transport Code, 2004. Version 5, LA-UR-03-1987.